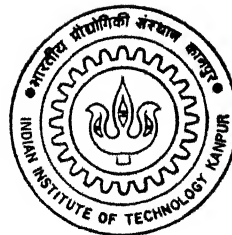# STUDIES ON SOURCE TO FIBRE COUPLING

by

ROOPAM GARG

DEPARTMENT OF ELECTRICAL ENGINEERING

INDIAN INSTITUTE OF TECHNOLOGY KANPUR

AUGUST, 1995

STUDIES ON SOURCE TO FIBRE COUPLING

A Thesis Submitted

in Partial Fulfilment of the Requirements

for the degree of

MASTER OF TECHNOLOGY

by

ROOPAM GARG

to the

DEPARTMENT OF ELECTRICAL ENGINEERING
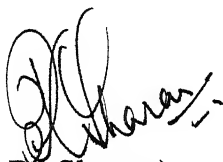
INDIAN INSTITUTE OF
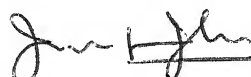
TECHNOLOGY KANPUR

August 1995

EE-1995-M-GAR-STU

Certificate

It is certified that the thesis entitled " *STUDIES ON SOURCE TO FIBRE COUPLING* " by ROOPAM GARG has been carried out under our supervision and that it has not been submitted elsewhere for the award of a degree.

(Dr. R. Sharan)
Professor
Dept. of Electrical Engg.
IIT Kanpur

(Dr. Joseph John)
Astt. Professor
Dept. of Electrical Engg.
IIT Kanpur

August 1995

Dedicated to

My Family

Acknowledgements

I express my deep sense of gratitude to Dr Joseph John for providing constant encouragement, valuable guidance, and keen interest during this work In spite of his busy schedule, he was always available to me I am indebted to Dr R Sharan for giving me an opportunity to work under his guidance and motivating me throughout the work.

I would like to thank Dr. P.R K Rao, Dr V. Sinha and Dr. R K Bansal for creating interest in my area of specialisation, communication systems

I am thankful to all of my friends for their help and kind suggestions I have no words to thank my senior Mr. Shyam Kishor and brother Shivam Garg for helping me in thesis preparation, despite their busy schedules I acknowledge the cheerful and warm company of all my M. Tech. batchmates, Rahul, Rajiv, Sanjay, Pavan, Jaipal and Ashish, for the moments that we shared together and made my stay memorable

Last, but not the least, I take this opportunity to convey my heartfelt gratitude to my parents, elder brother Anupam and sister Priyam, for their constant moral support and inspiration. I am very grateful to all my family members for their sacrifices Only because of their constant support and encouragement, I have been able to finish this work.

Roopam Garg

Abstract

Efficient coupling between source and fibre is a significant problem in optical fibre communication systems. An attempt has been made to study the basic couplings between source and fibre. The coupling problems of laser diode to single mode fibre is first considered. Hyperbolic microlenses are shown to be the ideal ones for the above problem. Coupling theory for these microlenses using various models are briefly presented, followed by comparison of results.

Coupling studies of light emitting diodes (LEDs) to multimode fibres are then considered. Far field patterns for source and fibres are obtained experimentally based on which a few parameters of LED and fibres are calculated. Various theoretical coupling models for this coupling problem are considered. Theoretical results are then compared with the measured results for a source and two types of fibres in a butt coupling configuration, using an optical glue, to improve the coupling efficiency. Measured results of these microlensed fibres are presented.

Contents

longitudinal offset

Summary

Chapter 5 : Conclusions and Suggestions for Future Work

References

List of Figures

LIST of TABLES

Chapter 1

Introduction

Light wave communication systems, using optical fibres as the communications medium are at present widely used in long haul and high information capacity applications. Because of the low-loss and high bandwidth transmission characteristics of optical fibres, these systems are ideally suited for carrying voice, data and video signals at extremely high rates over long distances. They have large non-repeated link spans. In addition, they offer other advantages as immunity to electromagnetic interferences, high reliability ensuring data security, low cross-talk, low weight and small dimensions of fibres etc A shift in the operating wavelength from 800 to 1300 nm allowed substantial increase in the repeaterless transmission distance for long haul systems. Single mode fibre systems promised lower losses and significantly larger bandwidth than the multimode fibres. Systems operating at 1500 nm provide the lowest attenuation but have much larger signal dispersion than at 1300 nm.

1.1 Optical Communication System

An optical fibre transmission link comprises of a transmitter consisting of a light source with its associated drive circuitry, optical fibre as the communication medium, and a receiver consisting of a photodetector plus amplification and signal-restoring circuitry. See fig.(1.1). Additional components may include optical connectors, splices, couplers, repeaters etc.

A light source is used to launch optical fibre into the fibre. Semiconductor light-emitting diodes (LEDs) and laser diodes are suitable transmitter sources as their light output can be modulated rapidly by simply varying the bias current. The transmitter circuitry converts electric signals into optical signals. This signal launched into the fibre gets attenuated and distorted with increasing distance in the waveguide, and is detected by the photodetector at the receiver end. The photodetector and optical source are square-law devices. Semiconductor pin and avalanche photodiodes are the two principal photodetectors used in a fibre optic links. The degraded signal received by the photodetector is amplified and reshaped.

TRANSMITTER

```
         ┌─────────────┐              ┌─────────────┐    optical
Electric │    Drive    │              │    Light    │    signal
         │   circuit   │─────────────▶│   source    │────────┐
input    │             │              │             │        │
signal   └─────────────┘              └─────────────┘        │
```

o
p
t
i
c
a
l

f
i
b
e
r

RECEIVER

```
Electric  ┌─────────────┐      ◁──      ┌──────────────┐
          │   Signal    │◀─────  ──────│ Photodetector│◀───
signal    │   restorer  │              │              │
out       └─────────────┘              └──────────────┘   optical
                          Amplifier                        signal
```
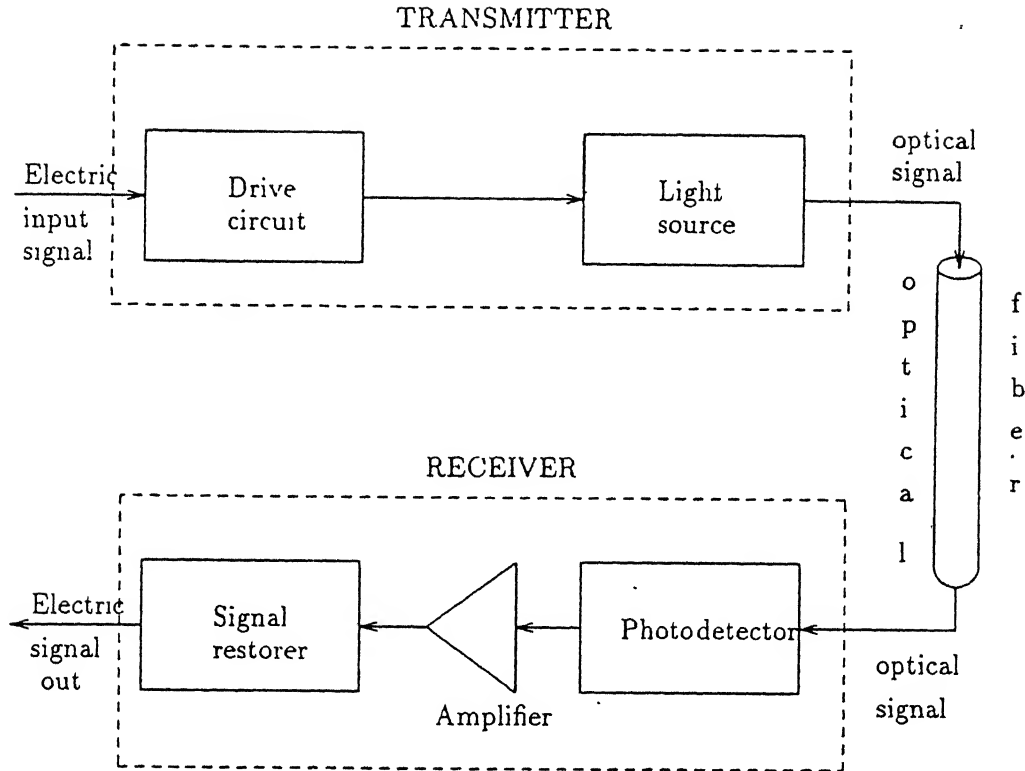
Figure 1.1: Basic configuration of an optical fiber transmission link.

1.2 Power Coupling and its Importance

In an efficient optical communication system, maximum possible power should be coupled between fibre, and source or detector. Power gets coupled in three stages-from light source to the fibre, from fibre to fibre and from fibre to detector. First one, viz. source to fibre, is very critical and decides maximum repeaterless spacing. It will be considered in our thesis in detail. However, highly efficient fibre to fibre coupling can be obtained using identical core radii and same numerical aperture. Also the coupling from fibre to photodetector is more easily accomplished than with light sources, because of their relatively larger active surface areas and large acceptance angles.

The coupling of optical fibre from a luminescent source into a fibre is influenced by the numerical aperture of fibre, the cross-sectional area of fibre core compared with the

2

source-emitting area, the radiance and spatial radiation pattern of the source. If the emitting area of source is smaller than the fibre core, then lensing schemes can be used to improve the source-fibre coupling efficiency. The NA mismatch between light source and fibre is the predominant cause of coupling loss. Due to highly directional emission beam and small emission area of lasers, coupling losses using lasers as light sources are smaller. In case of LEDs, higher coupling losses are due to the incompatibility between wide beam divergence of LEDs and the narrow acceptance cone of the fibre.

The power coupled from the source into a fibre is very critical in determining the maximum repeaterless spacing. Since the typical powers involved in a fibre optic system is very low, of the order of microwatts, a highly efficient source to fibre coupling scheme is required. Also source-fibre must be perfectly aligned because misalignments (offset or tilt) may adversely affect the coupling efficiency.

1.3 Objective of Present Work

As discussed in sec.1.2, highly efficient and stable source to fibre coupling is an important aspect in any fibre optic communication system. The main aim of this work is to study the source-fibre coupling theoretically for LD-SMF combination, and both theoretically and experimentally for LED-MMF combination. LD-SMF coupling theory for hyperbolic (ideal) microlenses is studied for longitudinal and lateral offsets.

Since both LED and MMF have a large number of modes having nonuniform power distribution among them, an exact calculation of coupling loss between them is lengthy and extremely complex. So we have tried to give simpler coupling theories for LED-MMF and compared them with the experimental results. Also effect of misalignments on coupling efficiency has been experimentally obtained. Microlenses are formed on the endfaces of multimode fibres and as expected they improve the power coupled into them by the source.

1.4 Overview

The thesis is organized in the following manner :
Chapter 2 begins with the description of basic laser diode to single mode fibre coupling problems. Mode theories are briefly discussed. Then coupling theory for ideal (hyperbolic) microlenses using finite-width phase shifter model and wave aberration model is discussed for

3

various offsets

Chapter 3 deals with the measurements and experiments on LED to MMF coupling Far field patterns of source and fibres (glass &plastic) are measured, and various parameters are obtained from them. Finally, microlenses are formed on MMFs. The results of direct and microlensed coupling for various offsets are compared.

Chapter 4 is devoted to the LED-MMF coupling theory. Three models - uniform modal power distribution of source, $\cos^m\theta$ and $\cos^n\phi$ distribution of source, and gaussian far-field pattern for fibre and source have been assumed. Experimental results are compared with the results using these models for longitudinal offset case.

Discussion of results and conclusions of work are included in chapter 5

In the end, a detailed list of reference used in this research work is given

CHAPTER - 2

LD-SMF Coupling Theory For Hyperbolic Microlenses

Since the advent of optical fibre communications, efficient coupling between laser source and optical fibre has been a problem of great concern for optimal performance of the system. Direct power coupling from laser source to single mode fibre is very small, typically 10% Coupling efficiency can be greatly improved by the formation of microlenses directly on the endfaces of fibres The lens serves to match the modes of the laser and fibre, ensuring maximum coupling when laser-fibre separation is finite. Thus the need to bring the two into physical contact is avoided. Microlenses formed on fibres generally posses automatic self-centering characteristic. This chapter is devoted to basic coupling problem between laser diode (LD) and single mode fibre (SMF), and also the use of microlenses to improve coupling efficiency. Theoretically, it is possible to collect nearly 100% of laser radiation with an aspheric lens design. Theoretical results on such ideal microlenses (hyperbolic microlenses) has been presented. LD-SMF coupling theory based on finite width phase shifter model and on wave aberration model for such microlenses is then presented. Finally maximum theoretical coupling efficiencies are compared, followed by misalignment studies.

2.1 Basic LD-SMF Coupling Problems

Coupling of light from a laser diode into a single mode optical fibre is a significant problem in the development of high speed, long haul optical communication systems. Over the last two decades, considerable research has gone into understanding the basic coupling problem, in order to achieve highly efficient coupling between laser diode and single mode fibre. A typical laser source emits light in one of several spatial modes. Most commonly used laser diodes are of edge-emitting type having rectangular light emitting region. The output beam from a laser diode diverges asymmetrically from the emitting surface, resulting in an elliptical as well as divergent beam profile. Also spot size of laser diode is very small (0.8-1.0 μm range). Spot size is defined as the beam radius at which amplitude of the approximated gaussian field for a laser

diode falls to 1/e of that at centre In contrast, single mode fibres have circular beam profiles with larger spot sizes and planar wavefronts Different spot sizes and wavefront nature of laser diode and single mode fibre result in high coupling losses. In order to achieve efficient coupling, both the spot sizes and wavefronts must be matched. An excellent solution for achieving high coupling is to use lenses between LD and SMF to match the beam parameters

2.2 Coupling Features

The standard coupling features are briefly discussed here, for the purpose of comparing different coupling schemes These are-

2.2.1 Coupling Efficiency

Coupling efficiency is defined as the fraction of the total optical source power that can be coupled into the fibre. It is a very important parameter for comparison of different coupling schemes In percentage, it is defined as,

$$Coupling\ efficiency\ (\%)\ =\ \frac{optical\ power\ coupled\ into\ fibre}{optical\ power\ emitted\ by\ a\ source} \times 100 \qquad (2.1)$$

Alternatively, coupling loss may be written in dB as,

$$Coupling\ Loss\ (dB)\ =\ 10\ \log_{10}\ (Coupling\ efficiency) \qquad (2.2)$$

It may also be termed as power coupling efficiency or power launching efficiency at source-fibre coupling. Higher the coupling efficiency, more efficient will be the coupling scheme.

2.2.2 Alignment Tolerance

It is defined as the amount of offset or tilt that produces 1 dB excess loss (or 80% of the maximum coupling efficiency) from the best aligned position. Offset may be longitudinal or lateral (axial). All the above three misalignments adversely affect the LD-SMF coupling efficiency High alignment tolerances are desirable.

2.2.3 Other Considerations

Optical feedback is the amount of light fed back to the laser cavity, mainly due to Fresnel reflections. It can be effectively reduced by using an optical isolator between source and fibre, or by antireflection coatings.

2.3 Mechanical Misalignments

Mechanical misalignment is one of the major problems in coupling light from source to fibre, as it adversely affects the coupling efficiency The three fundamental type of misalignments are discussed here briefly.

2.3.1 Longitudinal Offset-

Longitudinal offset occurs when two components of a fibre optic system have the same axis but have separation between their endfaces. This type of offset is very inherent in coupling because there always exist a gap between source-fibre, fibre-fibre and fibre-detector, in order to avoid the possible damage of endfaces of source and fibre. Longitudinal offset is illustrated in Fig.2 1(a).

2.3.2 Lateral Offset

Lateral offset results when the axis of the two components are separated by a distance 'd'. It is also called axial offset. Lateral offset is the most common misalignment occuring in practice and also causes the greatest power loss because of reduction in overlap area between two component endfaces, consequently reducing amount of optical power coupled. It has been illustrated in fig.2.1(b).
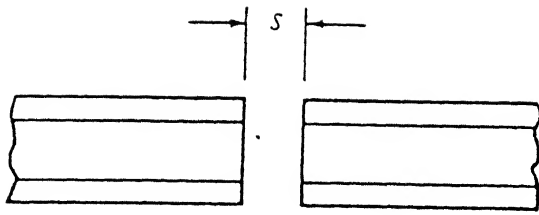
(a)   Longitudinal offset (end seperation)
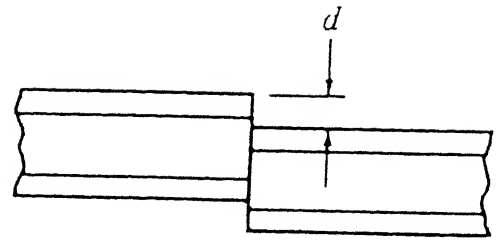
(b)   Lateral (axial) offset
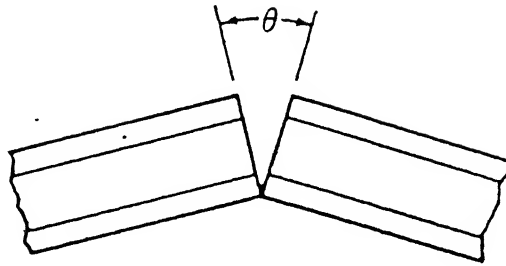
(c)   Angular offset (tilt)

Figure 2 1   Various types of mechanical misalignments between the fibres

2.3.3   Angular Offset (Tilt)

Angular offset occurs when the two axes (of fibre & source here) form an angle so that the component endfaces are no longer parallel. It may also pose a serious threat to the coupling efficiency Any angular offset can be expressed as the combination of above two offsets It has been shown in fig.2.1(c).

2.4   Mode Theories for LD & SMF

To understand the coupling between LD & SMF, the mode theory of laser diodes as well as that of step-index single-mode fibre   must be briefly discussed. Gaussian approximation for the LD beams and for the fundamental mode of the fibre has been assumed

8

For single or a few fibre modes, mode theory is preferred over the ray theory.

2.4.1 Mode Theory of Laser Diodes

The optical radiation in the laser diode is generated within a resonator cavity and sets up a pattern of electric and magnetic field lines, called the modes of the cavity. These can conveniently be separated into two independent sets of transverse electric (TE) and transverse magnetic (TM) modes. Each set of modes can be described in terms of the longitudinal, lateral and transverse half-sinusoidal variations of electromagnetic fields along the major axes of the cavity. The longitudinal modes are related to the length of the cavity and determine the principal structure of the frequency spectrum of the emitted optical radiation. Since length of the cavity is much larger than the lasing wavelength, many longitudinal modes may exist. Lateral modes describe the field distribution parallel to the junction plane. These modes depend on the side wall preparation and the width of the cavity, and determine the shape of lateral profile of laser beam. Transverse modes are associated with the electromagnetic field and beam profile in the direction perpendicular to the junction plane. These modes are of great importance, since they largely determine such laser characteristics as the radiation pattern (the angular distribution of the optical output power) and threshold current density. Lasing is the condition at which light amplification becomes possible in the laser diode and requires population inversion to be achieved. Cavity modes can be conveniently separated into two independent sets of transverse electric (TE) and transverse magnetic (TM) modes[10]. TE modes are generally favoured over TM modes due to their higher facet reflectivities

If d is the active layer thickness, n_1 and n_2 are the refractive indices of the active and cladding layer respectively, then the condition for single transverse mode (waveguide supporting the fundamental TE mode) is

$$d < \frac{\lambda}{2} \ (n_1^2 - n_2^2) \qquad\qquad (2.3)$$

where λ is the resonant wavelength of the laser diode.
Similarly, the condition for single lateral mode is

$$w < \frac{\lambda}{2} (n_{e1}^2 - n_{e2}^2)^{-\frac{1}{2}} \tag{2.4}$$

where w is the width of central region, n_{e1} and n_{e2} are effective indices of two regions.

2.4.2 Wave Nature of Laser Beams and Gaussian Approximation for Fundamental Mode

Wave nature of laser beams must be taken into account to understand gaussian approximation for the far-field distribution of laser diodes. Here we ignore the diffraction effects due to finite size of apertures.

Intensity distributions for laser beams are not uniform but concentrated near the axis of propagation and their phase fronts are slightly curved. A field component u of coherent light satisfies the scalar wave equation[11],

$$\nabla^2 u + k^2 u = 0 \tag{2.5}$$

where $k = 2\pi/\lambda$, is the propagation constant in the medium.
For light travelling in z-direction, one writes

$$u = \Psi(x,y,z) \exp(-jkz) \tag{2.6}$$

where ψ is slowly varying complex function which represents differences between laser beam and plane wave. By inserting eqn.(2.6) into eqn.(2.5) and neglecting term $\partial^2 \psi / \partial z^2$, we have

$$\frac{\partial^2 \Psi}{\partial x^2} + \frac{\partial^2 \Psi}{\partial y^2} - 2jk \frac{\partial \Psi}{\partial z} = 0 \tag{2.7}$$

Solution of the above differential equation is

$$\Psi = \exp(-j(P + \frac{k}{2q}r^2)) \qquad (2.8)$$

where $r^2 = x^2 + y^2$

The parameter P(z) represents a complex phase shift associated with the propagation of light beam, and q(z) is a complex beam parameter describing gaussian variation in beam intensity.

Eqn. (2.8) is called the fundamental gaussian beam solution Two real beam parameters R and w are related to the complex parameter q by

$$\frac{1}{q} = \frac{1}{R} - j\frac{\lambda}{\pi w^2} \qquad (2.9)$$

Inserting eqn. (2.9) in (2.8), we see the physical meaning, that R(z) is the radius of curvature of the wavefront that intersects the axis at z and w(z) is a measure of decrease of field amplitude with the distance from the axis. Intensity distribution is gaussian in every beam cross-section
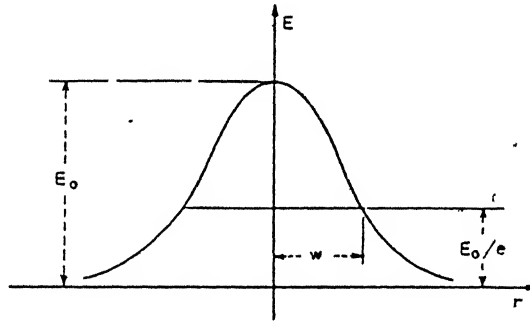
Fig.2.2 Amplitude distribution of the fundamental beam.

From fig.2.2, w is the distance at which amplitude is 1/e times that on axis and is often called the beam radius or spot size. Gaussian beam contracts to a minimum radius w_0 at the beam waist where the phase front is plane. The complex beam parameter at the waist is purely imaginary

$$q_0 = j \frac{\pi \, w_0^2}{\lambda} \qquad (2.10)$$

and at a distance z away from the waist of parameter is

$$q = q_0 + z = j \frac{\pi \, w_0^2}{\lambda} + z \qquad (2.11)$$

Combining eqns. (2.9) and (2.11), and separating real and imaginary parts, we obtain

$$w^2(z) = w_0^2 \left(1 + \left(\frac{\lambda z}{\pi w_0^2} \right)^2 \right) \qquad (2.12)$$

and

$$R(z) = z \left(1 + \left(\frac{\pi \, w_0^2}{\lambda \, z} \right)^2 \right) \qquad (2.13)$$

Fig.2.3 shows expansion of beam according to eqn. (2.12). The beam contour w(z) is a hyperbola with asymptotes inclined to the axis at an angle θ_{beam}, by putting,

$$\tan \theta_{beam} = \left(\frac{d \, w(z)}{dz} \right)_{z \to \infty} \qquad (2.14)$$

we get

$$\theta_{beam} = \tan^{-1} \left(\frac{\lambda}{\pi \, w_0} \right) \simeq \frac{\lambda}{\pi \, w_0} \qquad (2.15)$$

This is the far-field diffraction angle of the fundamental mode. The complex phase shift at a distance z is[11]

$$j \, P(z) = \ln \left(1 + \left(\frac{\lambda z}{\pi \, w_0^2} \right)^2 \right) - j \tan^{-1} \left(\frac{\lambda z}{\pi w_0^2} \right) \qquad (2.16)$$

So real part of P represents phase shift difference between gaussian beam and an ideal plane
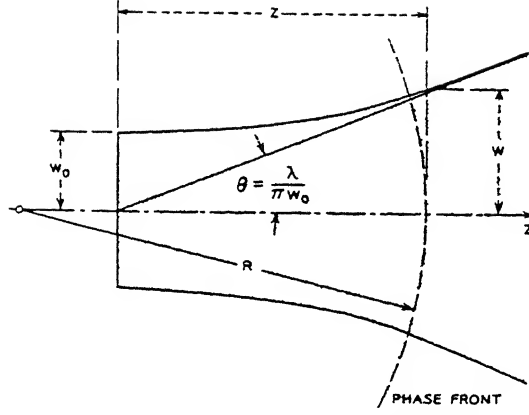
Fig.2.3 Contour of a Gaussian beam.

wave. Imaginary part produces amplitude factor w_0/w i.e. intensity decrease. Combining all the results for fundamental gaussian beam,

$$U\ (r,z)\ =\ \frac{w_0}{w}\ \exp\ (\ -j\ (kz\ -\ \Phi)\ -\ r^2\ (\frac{1}{w^2}\ +\ \frac{jk}{2R})\ )\qquad (2.17)$$

where $\phi(z)$ indicates an additional phase shift due to the geometry of the beam, and is given by

$$\Phi\ =\ \tan^{-1}(\frac{\lambda z}{\pi w_0^2}).\qquad (2.18)$$

In eqn. (2.15), θ_{beam} corresponds to half angle at $1/e$ of far field angular field distribution. Generally half of FWHM (Full width at half maximum) angle is used in the calculation of spot sizes, instead of θ_{beam}. $\theta_{1/2}$ in terms of θ_{beam} is

$$\theta_{1/2}\ =\ \theta_{beam}\ \sqrt{\frac{\ln(2)}{2}}\qquad (2.19)$$

13

Substituting θ_{beam} from eqn (2.18) we get,

$$\theta_{1/2} = \tan^{-1} \left(\frac{\lambda \sqrt{\ln(2) / 2}}{\pi \ w_0} \right) \qquad (2.20)$$

Hence spot-size is calculated as,

$$w_0 = \frac{\lambda \sqrt{\ln(2) / 2}}{\pi \ \tan(\theta_{1/2})} \qquad (2.21)$$

The spot-sizes may be used in the calculations of source-fibre coupling efficiency.

2.4.3 Mode Theory of Step index Single-mode Fibre

For good understanding of the optical power propagation mechanism in a fibre, it is necessary to solve Maxwell's equations subject to the boundary conditions of fibre.

Wave equations derived from Maxwell's equations are given by,

$$\nabla^2 E \ - \ \mu\varepsilon \ \frac{\partial^2 E}{\partial \ t^2} \ = \ 0 \qquad (2.22)$$

$$\nabla^2 H \ - \ \mu\varepsilon \ \frac{\partial^2 H}{\partial \ t^2} \ = \ 0 \qquad (2.23)$$

where μ and $\in$ are permeability and permittivity of medium respectively. If electro-magnetic waves propagate in z-direction and β is z-component of propagation vector We find mode solutions as

$$E = E_0 \ (r, \Phi) \ e^{j(\omega t - \beta z)} \qquad (2.24)$$

$$H = H_0 \ (r, \Phi) \ e^{j(\omega t - \beta z)} \qquad (2.25)$$

14

Wave equations in cylindrical co-ordinates are given as

$$\frac{\partial^2 E_z}{\partial r^2} + \frac{1}{r}\frac{\partial E_z}{\partial r} + \frac{1}{r^2}\frac{\partial^2 E_z}{\partial \phi^2} + q^2 E_z = 0 \qquad (2.26)$$

$$\frac{\partial^2 H_z}{\partial r^2} + \frac{1}{r}\frac{\partial H_z}{\partial r} + \frac{1}{r^2}\frac{\partial^2 E_z}{\partial \phi^2} + q^2 H_z = 0 \qquad (2.27)$$

If $E_z = 0$, modes are called transverse electric (TE),

If $H_z = 0$, modes are called transverse magnetic (TM) and

If both E_z & H_z exists, modes are hybrid (EH or HE).

we assume independent solutions for E_z (or H_z) as

$$E_z(\phi, r) = \phi(\phi)\ F(r) \qquad (2.28)$$

and modes of step-index optical fibre are solved in core and cladding regions of fibre. If wave is periodic function in time and propagates in z-direction, wave equation for E_z becomes

$$\frac{\partial^2 F(r)}{\partial r^2} + \frac{1}{r}\frac{\partial F(r)}{\partial r} + [\,q^2 - \frac{v^2}{r^2}]\ F(r) = 0 \qquad (2.29)$$

The above equation is known as differential equation for Bessel functions. For step-index fibre, we consider homogeneous core of refractive index n_1 and radius a, which is surrounded by infinitely thick cladding of index $n_2 < n_1$ such that guided modes in the core have exponentially decaying fields outside core. Also guided modes must remain finite as r $\rightarrow$ 0. This differential equation is solved using Bessel function in the core and modified Bessel function in the cladding. The cutoff condition i.e. the point at which a mode is no longer bound to the core region is

$$n_2\ k = k_2 \preceq \beta \preceq k_1 = n_1\ k \qquad (2.30)$$

where $k = 2\pi/\lambda$ is free space propagation constant.

An important parameter connected with the cutoff condition is the normalised frequency V (also called V number) defined by

$$V^2 = (\frac{2\pi a}{\lambda})^2 \, (n_1^2 - n_2^2)$$

(2.3

which is a dimensionless number that determines how many modes a fibre can support
specific mode can propagate only above its cutoff frequency. The fundamental mode i.e. LP_{01}
HE_{11} has no cutoff and can exist at any frequency.

Hence the condition for single-mode propagation is

$$V = \frac{2\Pi a}{\lambda} \, \sqrt{n_1^2 - n_2^2} \leq 2.405$$

(2.31

Core radius and refractive indices of core and cladding are appropriately chosen to satisfy abo
condition for single mode operation in optical fibres.

2.4.4   Gaussian Approximation for Fundamental Mode

It has been observed that fundamental mode intensity pattern and hence field distributio
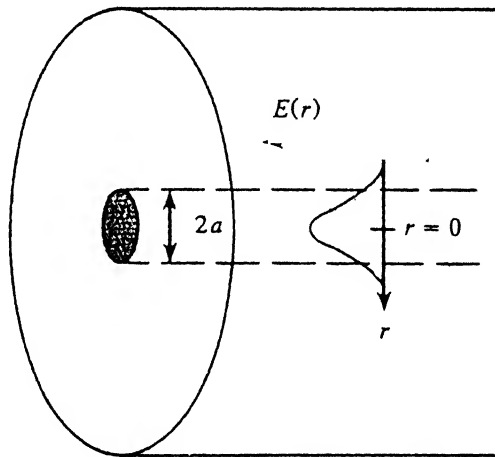
Figure 2.4   Field distribution in step-index single mode fibre

for a step-index single mode fibre is approximately Gaussian. A fundamental parameter of SMF is mode field diameter (MFD) and is determined from mode field distribution of fundamental mode. This mode field diameter is analogous to the core diameter in multimode fibres, except that in SMF not all the light which propagates through the fibre is carried in the core. Half of MFD is the spot size also defined as radius of beam at the beam waist.

So we can assume field distribution at distance r as

$$E(r) = E_0 \cdot \exp\left(-\frac{r^2}{W_f^2}\right)$$

where E_0 is field at zero radius.

2.5 Butt Coupling

Butt coupling is the simplest way to couple laser diode power into single mode fibre directly i.e. when there are no lenses between LD and SMF. When both laser and SMF beams are assumed Gaussian, and assuming no offset or tilt between LD & SMF, butt coupling coefficient is [12]

$$C_{butt} = \frac{4}{\left(\frac{W_0}{W_f} + \frac{W_f}{W_0}\right)^2 \left(1 + \left(\frac{2z}{k(W_0^2 + W_f^2)}\right)^2\right)} \tag{2.34}$$

where W_0 and W_f are spot sizes of laser beam and SMF fundamental mode respectively. z is LD-SMF seperation, Butt coupling yields very low coupling efficiency (less than 15%) , as shown in fig.2.5.

In our analysis, we have used the LD and SMF parameters given in table (2.1) and (2.2) respectively

Coupling efficiency when no optical component
between LD-source and SMF
(Butt Coupling)
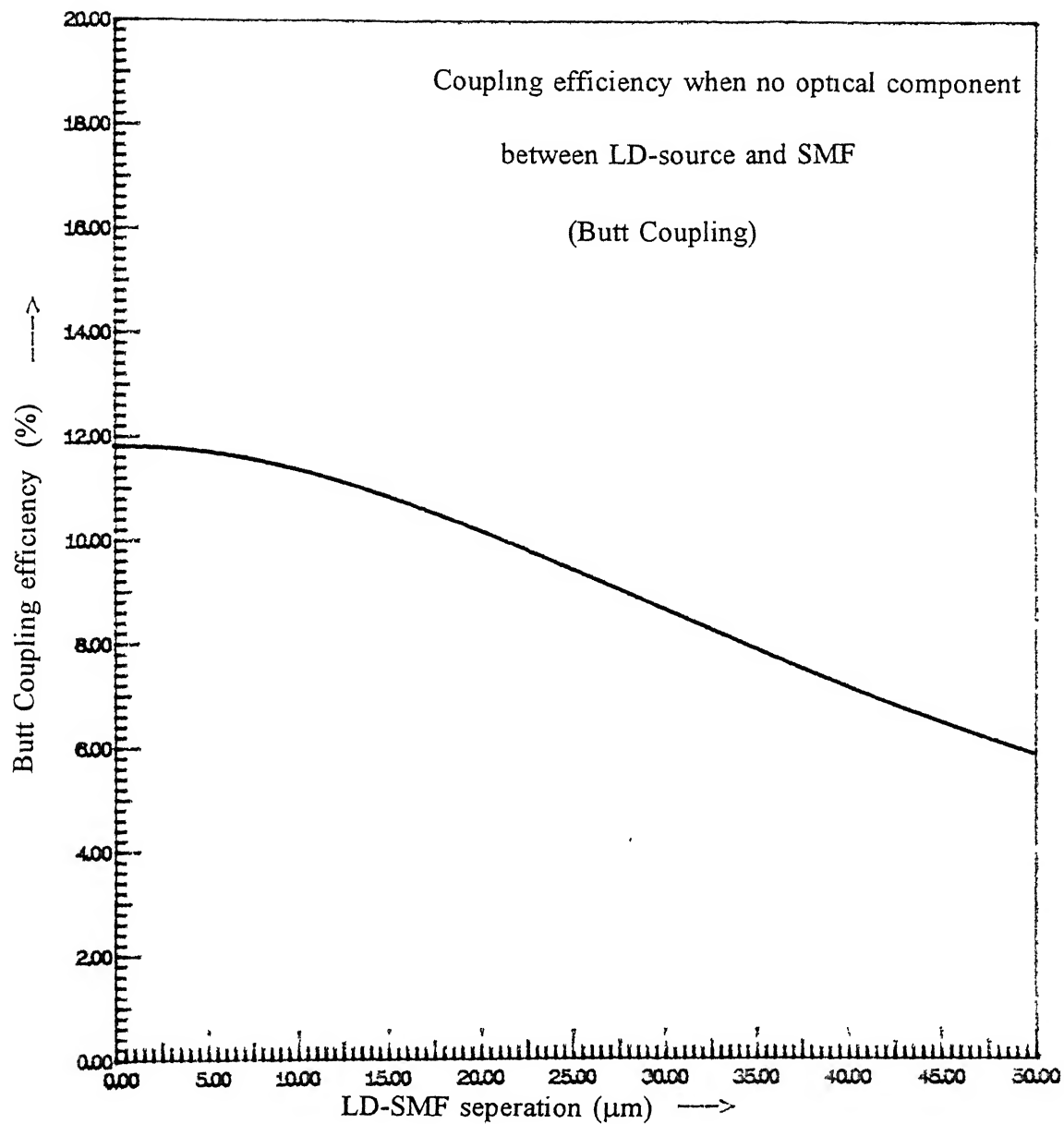
Figure 2.5 Butt coupling efficiency Vs longitudinal offset (LD-SMF seperation)

Table (2.1) LD Parameters

Wavelength (λ)	1.5 μm.
Spot-size in X-direction (W_{0x})	0.857 μm.
Spot-size in Y-direction (W_{0y})	0.843 μm.

Table (2.2) Conventional SMF Parameters

Core diameter (2a)	7.3 μm.
Spot-size (w_f)	4.794 μm.
Core refractive index (n_1)	1.461
Numerical aperture (NA)	0.126
V number at 1.5 μm.	1.924

From eqn. (2.34), it is clear that maximum coupling efficiency for particular LD-SMF combination occurs when z = 0 i.e. fibre is in contact with LD. Since laser diode facet is extremely sensitive to scratches, they may get damaged. So this is not practical. Also optical feedback will be more. Butt coupling is used for simplicity and for better alignment tolerance.

2.6   Lensed Coupling

In order to achieve efficient coupling between LD and SMF, both the spot sizes and phase fronts must be matched. An appropriate solution is to   use lenses between LD and SMF. This can be understood in the following way. Total butt coupling loss (L_{tot}) has been shown in fig.2.6 and is the sum of spot size (L_{ss}) and phase front mismatch loss (L_{ph}) .

18
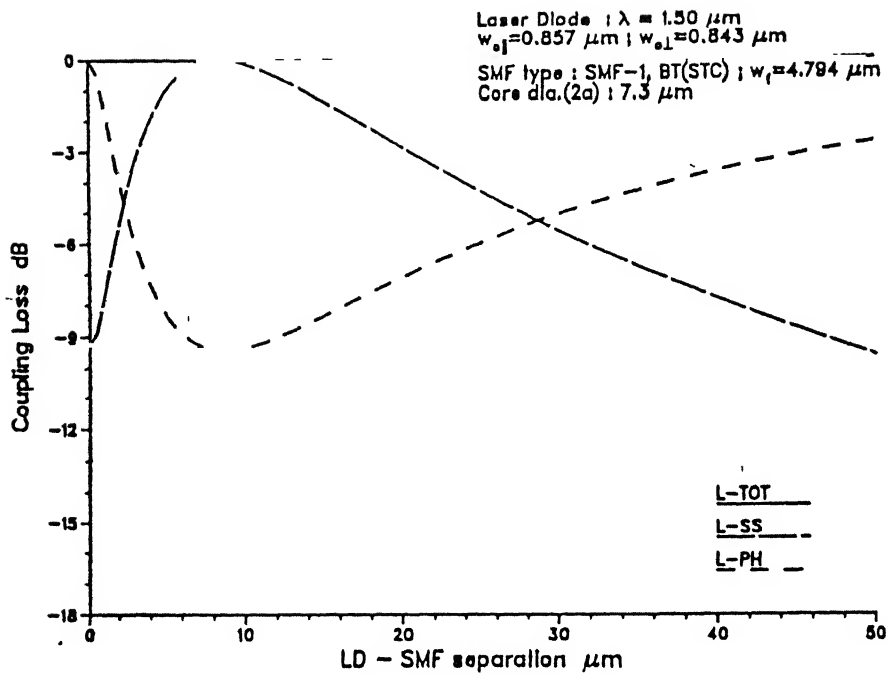
Fig. 2.6   Components of the total butt coupling loss (L—TOT) :
a) Spot size mismatch loss (L—SS)
b) Phase mismatch loss (L—PH)

To minimize total coupling loss, zero LD-SMF seperation is avoided due to possible damage of extremely sensitive LD facet & finely cleaved SMF endface. So we try to match the phase front where the spot size mismatch loss tends to zero. It can be achieved using lenses between LD and SMF. Lensed coupling thus offers higher coupling efficiency than butt coupling. Also, maximum efficiency is obtained when SMF is placed at some finite distance from the LD

2.6.1 Coupling Using Discrete Lenses

In order to get higher coupling efficiency using discrete lenses, many lenses as cylindrical, spherical, conical, graded-index etc. and their combinations have been used. The efficiencies upto 80% have been actually obtained. Discrepency mainly lies due to assuming ideal lens while practically, lens aberration is one of the dominating factor that increases the coupling loss. Such

19

systems also suffer from critical alignment tolerances.

2.6.2   Coupling Using Microlenses

Reduction of coupling loss using discrete lenses require very precise alignment of laser, lens and SMF Alignment tolerances are slightly relaxed when a microlens is fabricated directly on the tip of fibre. Microlenses having true self-centering characteristics have been fabricated. They are minute in size and have small lens radius of curvature. Since no external lens is necessary, only a single alignment step is required. However, they suffer from poor alignment tolerance and complex microlens fabrication techniques.

2.7   Suitability of Hyperbolic Microlenses as the Ideal Lenses

The major aim of studying LD-SMF coupling is to investigate the means by which coupling efficiency should be made close to 100%. Direct coupling from laser diode to single-mode fibre yields poor coupling efficiency ($\approx$10-15%) while using discrete lenses between them to improve the coupling efficiency suffer from very poor alignment tolerance of the whole system. It has been shown earlier that, in spite of small alignment tolerance, lenses formed on the endfaces of fibres (microlenses) are preferred. Ball and Grin rod lenses when used in coupling increase efficiency only marginally. The spherical aberration of the lenses contributes very strongly to the coupling losses and limits the maximum coupling efficiency. In lensed coupling, losses occur due to Fresnel reflections, beam truncation by finite lens aperture and spherical aberration resulting from variation in optical path lengths from focal point to lens to a given planar wave front.

Requirements for an ideal lens shape[18] are :

1. It should have aperture large enough to collect all laser radiation.

2. It should be free of spherical aberration.

3. It should have focal length that perfectly matches the laser and fibre modes.

4. It should be appropriately coated to eliminate reflections.

It has been shown that a hyperbolic lens shape is free of spherical aberration for a particular design i.e. all optical path lengths from a given wave front to the focus are equal.

Hyperbolic lens parameter for this shape are given by eqn (2.48) and (2.49). It also does not suffer from a limited aperture for typical lasers when matching the laser and fibre modes. Now by using anti-reflection coatings, Fresnel's reflections can be avoided. We see thus that all the conditions of ideal microlens are satisfied for hyperbolic microlens. In our analysis, we will consider this particular design of hyperbolic microlenses. Hence it is theoretically possible to collect 100% radiation using aspheric (hyperbolic) lens design. The construction of a hyperbolic microlens on the endface of a single-mode fibre presents constructional difficulties. However, these have recently been overcome using laser micromachining techniques[17]. Recently Edwards and Presby[18] have given experimental coupling efficiency of 90% using hyperbolic microlenses. This efficiency is stated to have been optimized and occurs for a particular value of focal length. Although this theoretical model predicts 100% efficiency for optimum focal length, the experimental value of 90% achieved without coating represents highest known coupling efficiency of any matching device so far.

2.8 LD - SMF Coupling Theory for Hyperbolic Microlenses

The LD and SMF fields are assumed to be gaussian. So LD tangential field (normalized to unit power) at a distance L from the LD facet is written as[12]

$$F_{LD}(x,y) = [\frac{2}{\Pi\ W_x\ W_y}]^{\frac{1}{2}} \exp(-\frac{x^2}{W_x^2} - \frac{j\ k\ x^2}{2R_x} - \frac{y^2}{W_y^2} - \frac{j\ k\ y^2}{2R_y}) \qquad (2.35)$$

where W_x and W_y are spot sizes at distance L from the LD facet in x-z and y-z planes respectively. Corresponding waist spot sizes are W_{0X} and W_{0Y} . So

$$W_x^2\ =\ W_{ox}^2\ [\ 1\ +\ (\frac{2\ L}{k\ W_{ox}^2})^2] \qquad (2.36)$$

$$R_x\ =\ L\ [\ 1\ +\ (\frac{k\ W_{ox}^2}{2\ L})^2\ ] \qquad (2.37)$$

$$W_y^2 = W_{oy}^2 [1 + (\frac{2L}{k W_{oy}^2})^2] \qquad (2.38)$$

$$R_y = L [1 + (\frac{k W_{oy}^2}{2L})^2] \qquad (2.39)$$

Here we have assumed perfect transverse and angular alignment between LD and SMF, and also that a circularly symmetric microlens is formed on SMF endface. So normalised tangential field of microlensed SMF is given as

$$F_{fib}(x,y) = (\frac{2}{\Pi})^{\frac{1}{2}} \frac{1}{W_{fib}} \exp[- \frac{r^2}{W_{fib}^2} + j \phi(r)] \qquad (2.40)$$

where $r = (x^2 + y^2)^{1/2}$ and $\phi(r)$ is the phase shift introduced by the microlens. Microlens action has been assumed to be merely phase shifting and hence the transmission coefficient,

$$T_{ML} = \exp[+j \phi(r)] \qquad (2.41)$$

So power Coupling Coefficient is written as

$$\eta = \frac{4}{\Pi^2 W_x W_y W_{fib}^2} [A_1^2 + A_2^2] \qquad (2.42)$$

where

22

$$A_1 = \int\limits_{-\infty}^{+\infty} \int\limits_{-\infty}^{+\infty} \exp[-Re\ (x,y)]\quad \cos\ [Im\ (x,y)\ ]\quad dx\ dy \tag{2.43}$$

$$A_2 = \int\limits_{-\infty}^{+\infty} \int\limits_{-\infty}^{+\infty} \exp[-Re\ (x,y)]\quad \sin\ [Im\ (x,y)\ ]\quad dx\ dy \tag{2.44}$$

$$Re\ (x,y)\ =\ \frac{x^2}{W_x^2}\ +\ \frac{y^2}{W_y^2}\ +\ \frac{x^2+y^2}{W_{fib}^2} \tag{2.45}$$

$$Im\ (x,y)\ =\ k\ [\ \frac{x^2}{2\ R_x}\ +\ \frac{y^2}{2\ R_y}\ ]\ +\ \phi(r) \tag{2.46}$$

The integrals for evaluating A_1 and A_2 can be computed numerically using NAG (Numerical Algorithm group) subroutines. Microlens phase shift can be obtained by considering two models finite-width phase shifter model and wave aberration model.

2.8.1 For Finite-width Phase Shifter Model (FWPS-Model)

In this model, we have assumed the microlenses to be thin lenses of finite width and acting as mere phase shifters. These phase shifts introduced depend on the shape of microlens. All the microlenses have been assumed to be perfectly radially symmetric. Total phase shift $\phi_{hyp}(r)$ is phase shift through the lens and through the air, surrounding the lens before LD beam reaching the SMF endface. From fig.2.7, if D(r) is the distance from the lens vertex to a plane of radial dimension r within lens, then for hyperbolic lenses, we can write

$$\frac{(D(r)\ +\ A_{hyp})^2}{A_{hyp}^2}\ -\ \frac{r^2}{B_{hyp}^2}\ =\ 1 \tag{2.47}$$

where A_{hyp} and B_{hyp} are constants of the hyperbola.

For the ideal lens shape to be described as hyperbolic, all the rays converge at the focus in phase
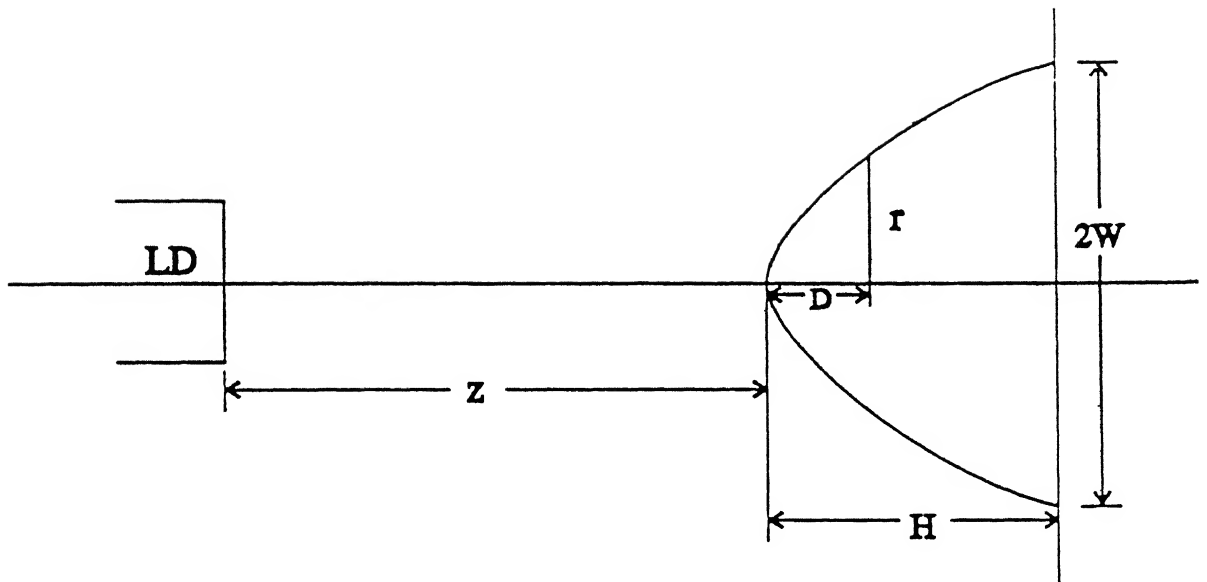
Figure 2.7 Hyperbolic Microlens : Geometry for the Finite-width Phase Shifter Model
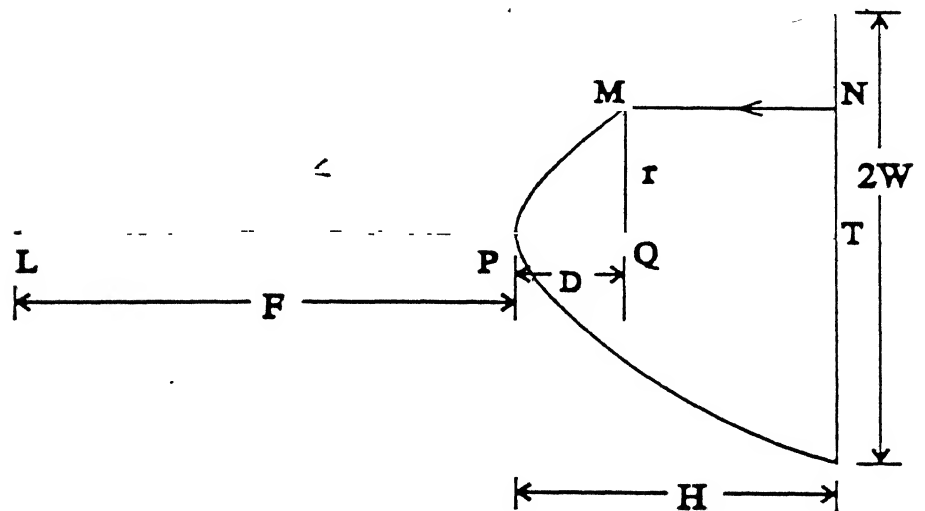
Figure 2.8 An Ideal Hyperbolic Microlens

and hence is free of spherical aberration See fig .(2.8). So constant A_{hyp} and B_{hyp} can be expressed in terms of focal length of lens F_{hyp} and refractive index of microlens n as given be Edwards and Presby[18]

$$A_{hyp} = (\frac{1}{n+1}) \ F_{hyp} \tag{2.48}$$

$$B_{hyp} = (\frac{n-1}{n+1})^{\frac{1}{2}} \ F_{hyp} \tag{2.49}$$

Total phase shift = phase shift through air + phase shift through the lens

$$\Phi_{hyp}(r) = k \ (D(r) + n \ (H_{max} - D(r))) \tag{2.50}$$

where H_{max} is the maximum height of hyperbolic lens, and n is the refractive index of microlens. Also $D(r)$ is given from eqn. (2.47) .

Coupling efficiency calculations are carried out for this model with the phase shift given by eqn. (2.50) and theory in section (2.8). Results are obtained by simulating it through a simple program for different values of LD-SMF seperation and focal length, and optimum values are obtained. Results have been discussed later in this chapter.

2.8.2 For Wave Aberration Model (WABR-Model)

In this model, the total phase shift by the hyperbolic microlens is obtained in terms of wave aberration. Wave aberration is the optical path difference between actual wavefront and flat reference wavefront, behind the lens and perpendicular to the fibre axis. Consider fig.2.9 with meridional ray from laser source. SV is the reference plane and Z is seperation distance between LD and lens vertex, so maximum slope angle is

$$\theta_{max} = \tan^{-1} (\frac{W_{max}}{Z + H_{max}}) \tag{2.51}$$

where H_{max} and W_{max} are maximum lens height and half maximum lens width respectively.

For typical ray LM, total optical path length upto the reference plane is

where n is refractive index of lens material LM can be written as,
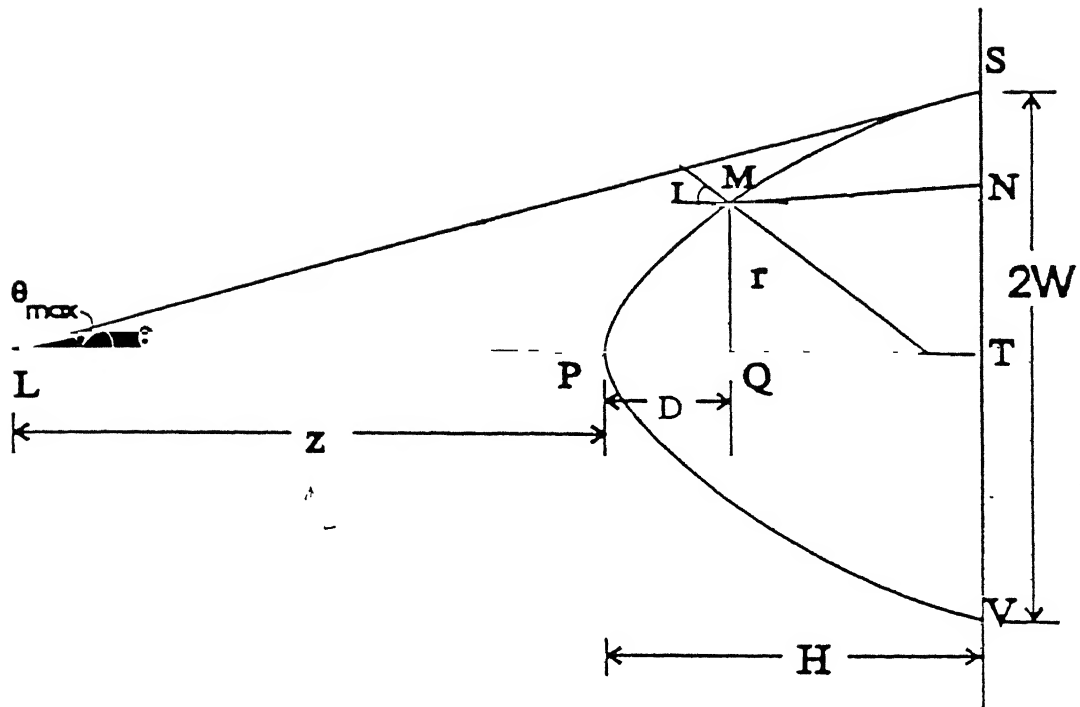
Figure 2.9 Hyperbolic Microlens : Geometry for the
Wave aberration Model
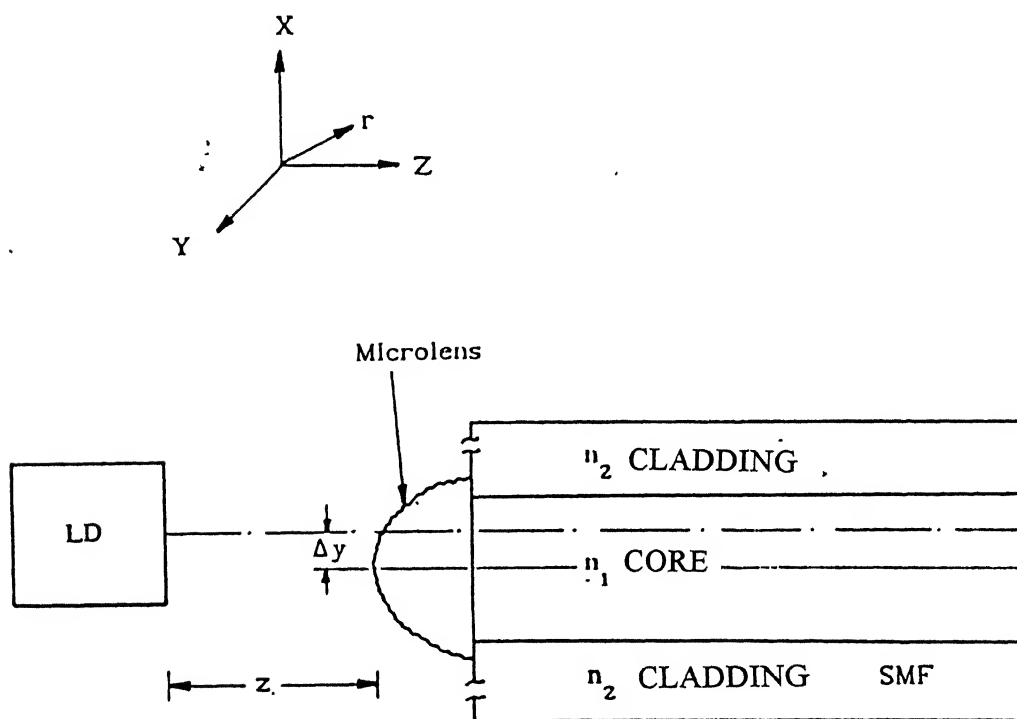
Fig. 2.10   LD-Microlensed SMF Configuration in the presence of
Transverse Offsets

$$OPL \ (LN) \ = \ LM \ + \ n \ MN \qquad (2.52)$$

$$LM \ = \ \sqrt{(\ Z \ + \ D(r)\ )^2 \ + \ r^2} \qquad (2.53)$$

$$D(r) \ = \ \frac{A_{hyp}}{B_{hyp}} \ (\sqrt{B_{hyp}^{\ 2} \ + \ r^2} \ - \ B_{hyp}) \qquad (2.54)$$

Let θ_i and I_i are slope and incident angles and θ_r and I_r are the angles after refraction respectively, then by geometry,

$$\theta_i \ = \ \tan^{-1} \ (\frac{r}{Z \ + \ D(r)}) \qquad (2.55)$$

$$(I_i \ + \ \theta_i) \ = \ \tan^{-1} \ (slope \ of \ normal \ i.e. \ \frac{d \ D(r)}{dr}) $$

$$= \ \tan^{-1} \ (\frac{A_{hyp} \ r}{B_{hyp} \ \sqrt{B_{hyp}^{\ 2} \ + \ r^2}}) \qquad (2.56)$$

$$\sin I_r \ = \ \frac{(\ \sin I\ )}{n} \qquad (2.57)$$

$$\theta_r \ = \ \theta_i \ + \ I_i \ - \ I_r \qquad (2.58)$$

$$MN \ = \ \frac{(\ H_{max} \ - \ D(r))}{\cos \theta_r} \qquad (2.59)$$

25

Also optical path length for flat reference wavefront is

$$OPL\ (LT)\ =\ z\ +\ n\ H \tag{2.60}$$

So wave aberration $E_{HYP}(r)$ is

$$E_{HYP}(r)\ =\ OPL\ (LT)\ -\ OPL\ (LN) \tag{2.61}$$

Hence the phase shift introduced by this lens model,

$$\Phi_{hyp}(r)\ =\ k\ E_{HYP}(r) \tag{2.62}$$

Theoretical computations for coupling efficiency for this model are carried out using above expressions and phase shift given eqn. (2.62). Results have been shown later in this chapter.

2.8.3 Modification for Misalignments

As shown earlier, there are three types of fundamental misalignments - longitudinal offset (source-fibre separation), lateral offset (axial separation) and angular offset (tilt). Here only first two have been considered as third can be expressed in other two. LD-SMF theory in section (2.8) is modified slightly for misalignments.

Let Δx and Δy are the misalignments in x and y direction. So now r becomes,

$$r_L\ =\ \sqrt{(x\ +\ \Delta x)^2\ +\ (y\ +\ \Delta y)^2} \tag{2.63}$$

and tangential field of microlensed SMF is

$$F_{fib}(x,y)\ =\ (\frac{2}{\pi})^{\frac{1}{2}}\ \frac{1}{W_{fib}}\ \exp\ (-\frac{(x\ +\ \Delta x)^2}{W_{fib}^2}\ -\ \frac{(y\ +\ \Delta y)^2}{W_{fib}^2}\ +\ j\ \Phi(r_L)) \tag{2.64}$$

For such misalignments, eqns. (2.42) to (2.44) remain the same but now Re(x,y) and Im(x,y) are given by

$$Re(x,y) = \frac{x^2}{W_x^2} + \frac{y^2}{W_y^2} + \frac{(x + \Delta x)^2 + (y + \Delta y)^2}{W_{fib}^2} \qquad (2.65)$$

$$Im(x,y) = k(\frac{x^2}{2R_x} + \frac{y^2}{2R_y}) + \Phi(r_L) \qquad (2.66)$$

Coupling results for x and y-direction offsets can be calculated using above expressions. Results are discussed later in the section

Kimura Model

This model[19] is based on paraxial ray theory approximation and can be assumed to be applied for infinitely wide lenses Gaussian fields are used to describe the modal fields of semiconductor laser diode and single-mode fibre. Optical absorption and surface reflection of the lens are neglected. We are presenting this model briefly here. Let η_x and η_y represent the contributions of the x and y components for coupling efficiency Then total coupling efficiency will be given by

$$\eta = \eta_x \eta_y \qquad (2.67)$$

where

$$\eta_x = \eta_{z,x} \, \eta_{d,z,x} \qquad (2.68)$$

$$\eta_{z,x} = \frac{\frac{2}{W_f . W_x}}{[P^2 + Q^2]^{\frac{1}{2}}} \qquad (2.69)$$

$$\eta_{d,z,x} = Exp \left[-2 . d^2 .\left[\frac{1}{W_f^2} - \frac{P[\frac{1}{W_f^4} - \frac{(n-1) \, k}{2.R}] - Q [\frac{(n-1)k}{W_f R}]}{P^2 + Q^2}\right]\right] \qquad (2.70)$$
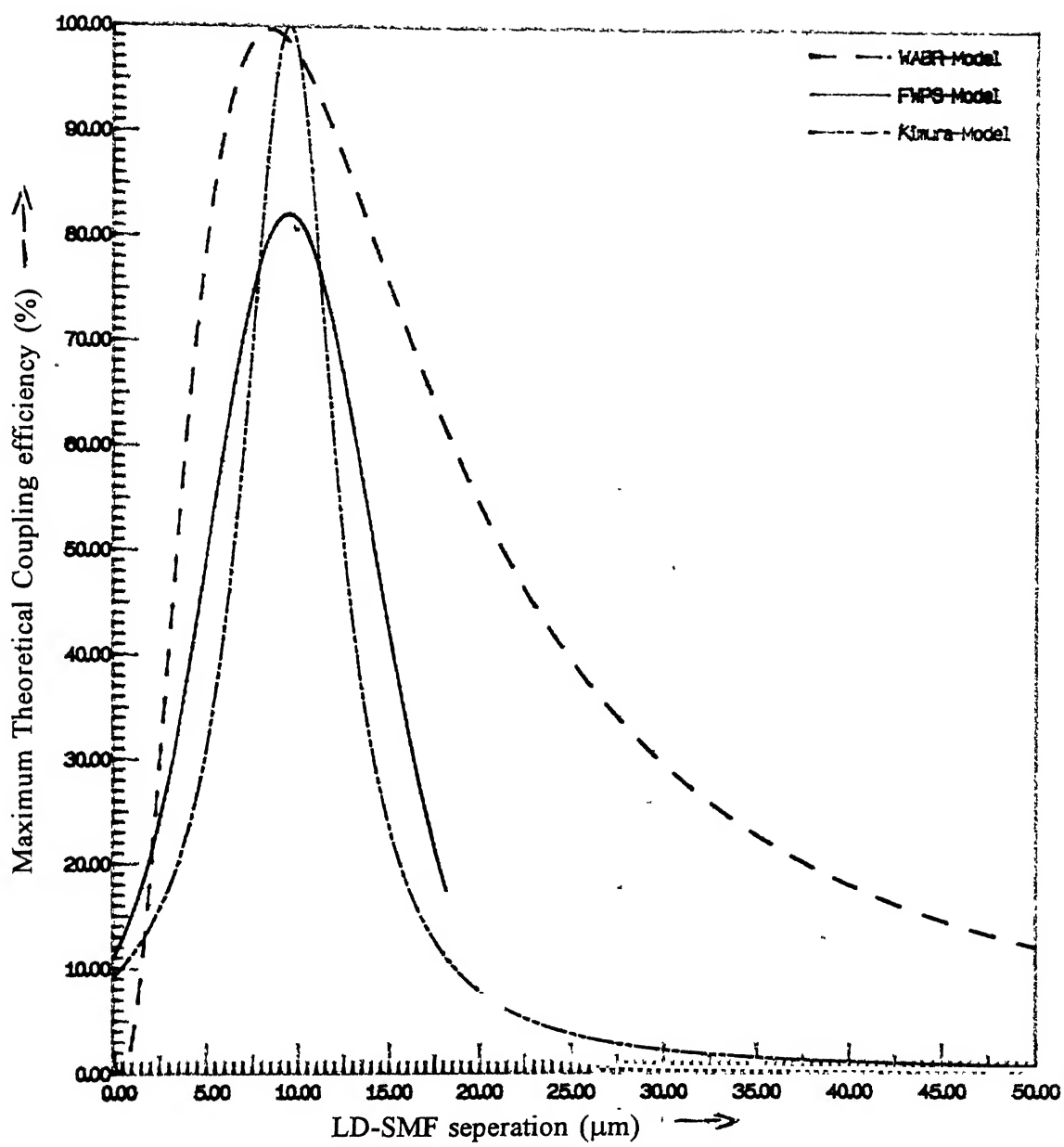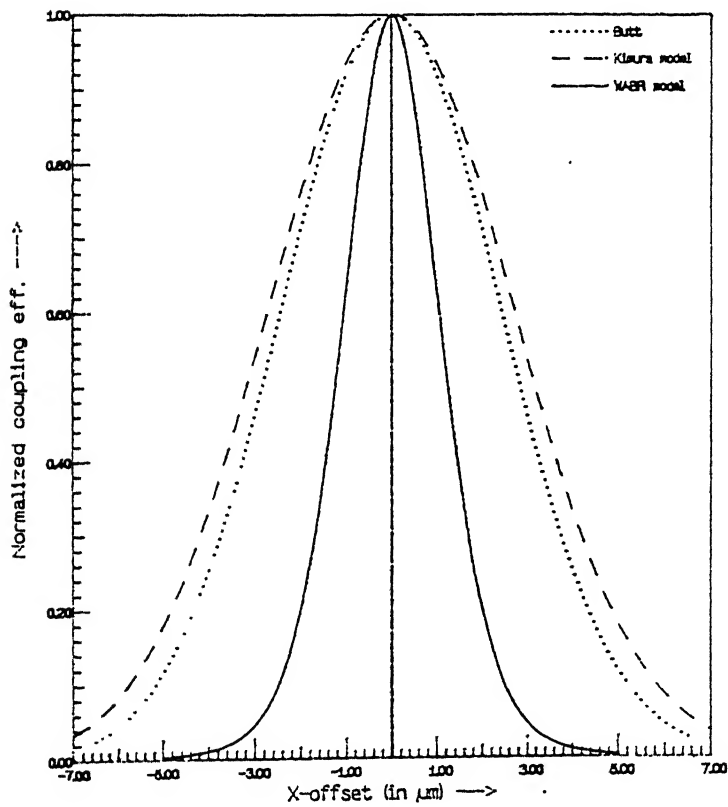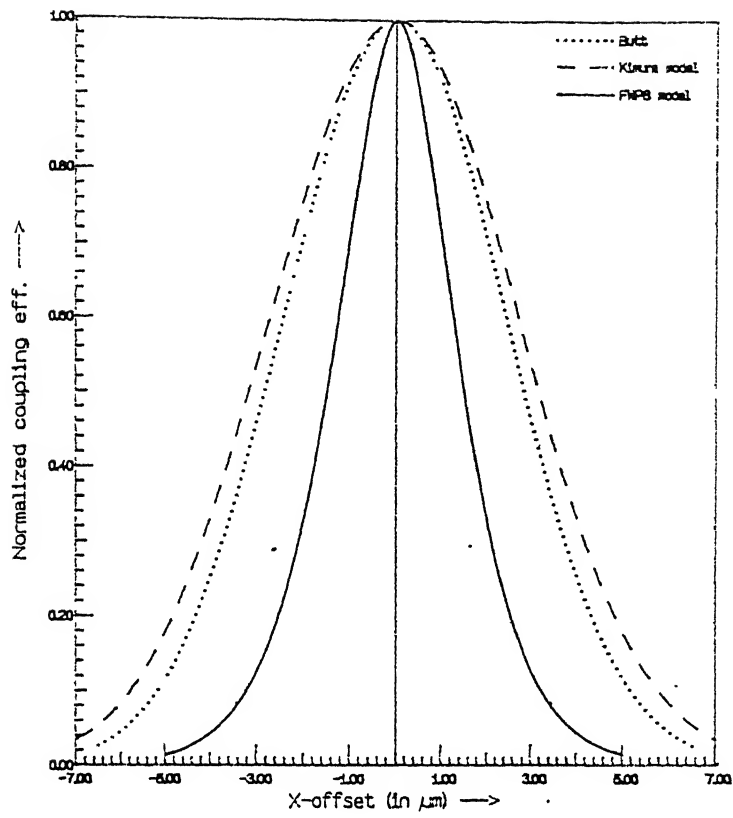
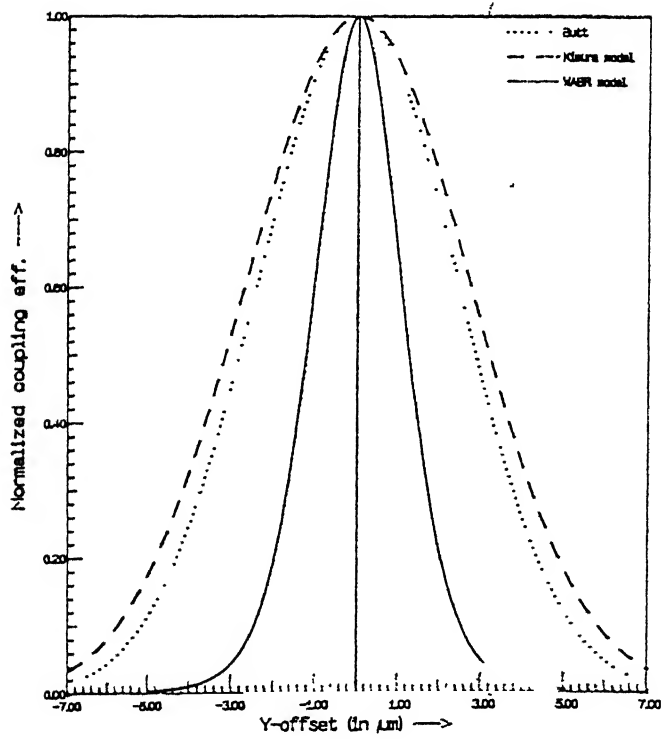Figure 2.11   Comparison of maximum theoretical coupling efficiency for longitudinal offset
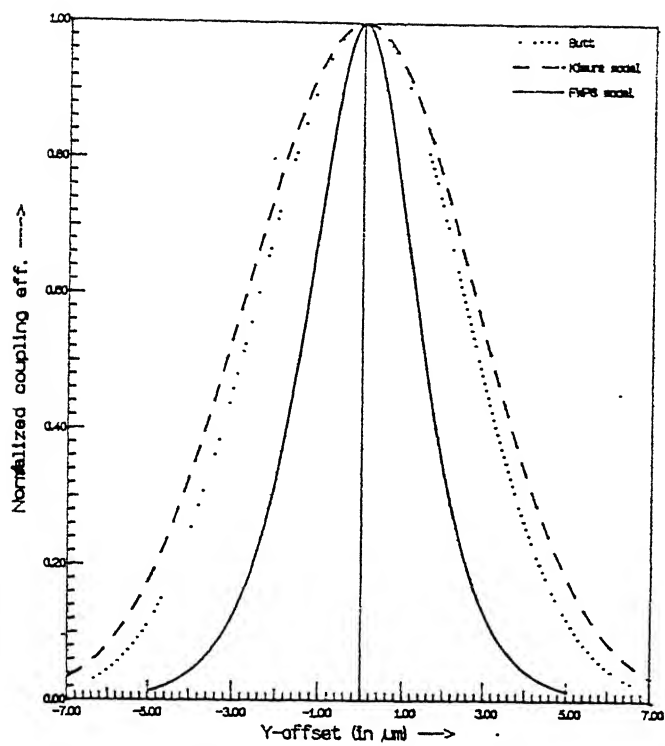
Fi

Figure. 2.13   Comparison of normalized coupling efficiency variations for Y-offset

where

$$P = \frac{1}{W_x^2} + \frac{1}{W_f^2} \qquad (2.71)$$

$$Q = \frac{K}{2.R_x} - \frac{(n-1).K}{2.R} \qquad (2.72)$$

where $\eta_{z,x}$ stands for coupling efficiency with longitudinal misalignment z and $\eta_{d,z,x}$ indicates the effect of z and giving lateral offset d . n and R are the refractive index and radius of curvature of the lens respectively . W_x , W_y , R_x , R_y are given by eqns (2.36) - (2.39).

When the lens is absent , put n = 1 and the above expression will reduce to the earlier butt coupling one, given by eqn. (2.34)

2.9 Comparison of Results for Various Offsets

Theoretical computations of LD-SMF coupling with hyperbolic microlenses are carried out using finite width phase shifter model (FWPS-Model) and wave aberration model (WABR-model). We have used LD and SMF parameters of table (2.1) and (2.2) respectively. The focal length of hyperbolic microlenses is varied in small increments from 0.1 to 50 μm, and corresponding hyperbolic constants A_{hyp} and B_{hyp} are calculated using eqn.(2.48) and (2.49) For each focal length, LD-SMF separation (z in μm) is varied from 0 to 50 μm. Optimal coupling efficiency for FWPS model is achieved as 82.03% at focal length 5 47 μm and at a distance z = 9.44 μm from LD source, whereas WABR model predicts 99.63% efficiency at LD-SMF separation (longitudinal offset) of 8.4 μm. See fig.(2.11). We have used a microlens half width of 20 μm in all our simulations and corresponding lens height is calculated using eqn.(2 54) for r = 20 μm. Maximum theoretical butt coupling efficiency is found to be 11.82% at z = 0. Kimura's results are also included in our comparison. It gives maximum theoretical coupling efficiency of 99 99% at 9.48 μm separation. Kimura has assumed infinite thick microlenses, which are impractical to assume. Hence from comparisons, it is clear that for longitudinal offset, thin lens assumption is not quite good We see that FWPS model is not the ideal choice for wide microlenses as hyperbolic microlenses.

To find the effect of lateral offsets on coupling results, we assume that the LD-SMF

separation is such that it gives maximum theoretical coupling efficiency Now lateral offsets are given in small increments in both directions and normalized coupling efficiencies are plotted. See fig (2.12) and (2.13). Alignment tolerance (axial offset producing 1 dB extra loss ≈80% of maximum coupling efficiency) is calculated for each model. They are 1.6 μm for butt coupling, 0 79 μm for FWPS model. Kimura's theory predicts the highest tolerance, while WABR model predicts the least. Since Kimura's theory assumes infinitely wide lenses, it is thought that his results are too optimistic. So wave aberration theory is more suited for hyperbolic microlens. In all the cases we have neglected the Fresnel reflection loss for which is around 4%. Since experimental data on these types of microlenses are not available, the validity of these models for lateral offsets could not be confirmed.

Summary

LD-SMF coupling theory for Ideal (Hyperbolic) microlenses has been discussed in this chapter. Starting with basic LD-SMF coupling problems and coupling features, mode theories for LD and SMF, and their gaussian beam fundamental mode assumptions have been given. Butt coupling results show lower coupling efficiencies. Efficiency is improved using lenses between LD and SMF. Hyperbolic microlenses are found to be the ideal ones. For these lenses, coupling theory using finite width phase shifter model and Wave aberration model have been given. These models are applied for coupling with presence of offsets. Kimura's results are found to be too optimistic. For Hyperbolic microlenses, WABR model is found to be better than others.

CHAPTER - 3

Measurements & Experiments on LED to MMF Coupling

Launching optical power from a source into a fibre entails considerations such as the numerical aperture, core size, refractive index profile, and core cladding index difference of the fibre, plus the size, radiance and angular power distribution of optical source. This chapter is devoted to measurement of source far-field radiation pattern and fibre characteristics such as numerical aperture and emission half angle. Results obtained by experiments are then compared with the theoretical ones. Lastly measured results of the improvement of coupling efficiency using microlenses, formed on the MMF endfaces have been shown. A comparative study of alignment tolerance for various misalignments have been made.

3.1 Measurement of Far Field Radiation Pattern of LED

The optical power that can be coupled into a fibre depends on the radiance, which is defined as the optical power radiated into a unit solid angle per unit emitting surface area. To determine the optical power-accepting capability of a fibre, spatial radiation pattern of the source must first be known. We consider a spherical coordinate system characterized by r, θ, ϕ with the normal to the emitting surface being the polar axis as Fig (3.1). Radiance of LED may be a function of both θ and ϕ. The emission pattern of a LED follows the relation,

$$B(\theta) = B(0) \cos^m \theta \qquad (3.1)$$

$$B(\Phi) = B(0) \cos^n \Phi \qquad (3.2)$$

For the LED in our experiments, the values of m and n were not available, necessitating experimental measurements.
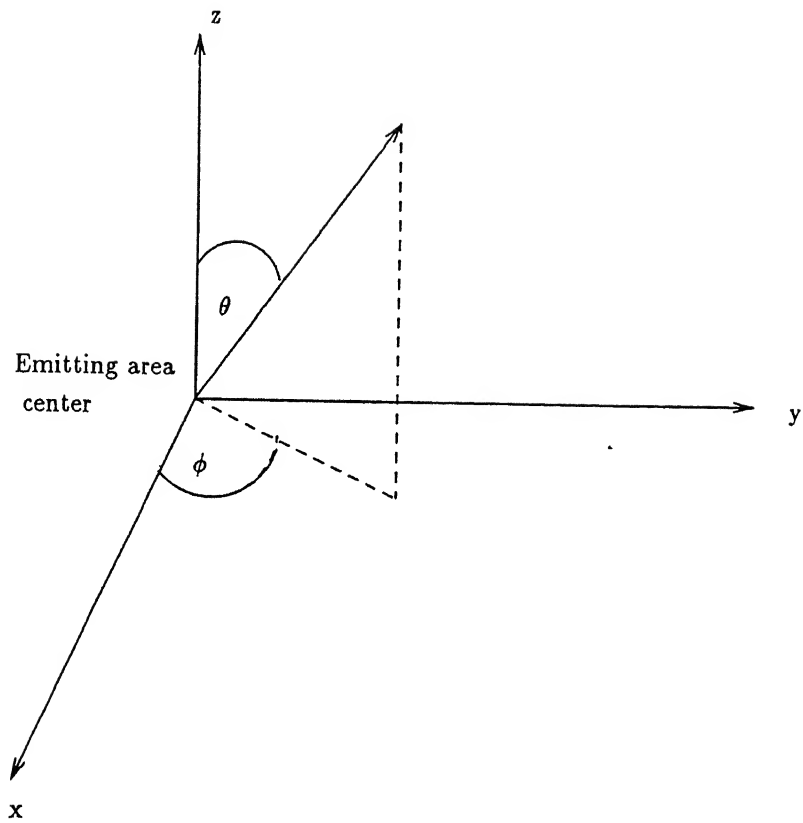
Figure 3.1 Spherical Coordinate system

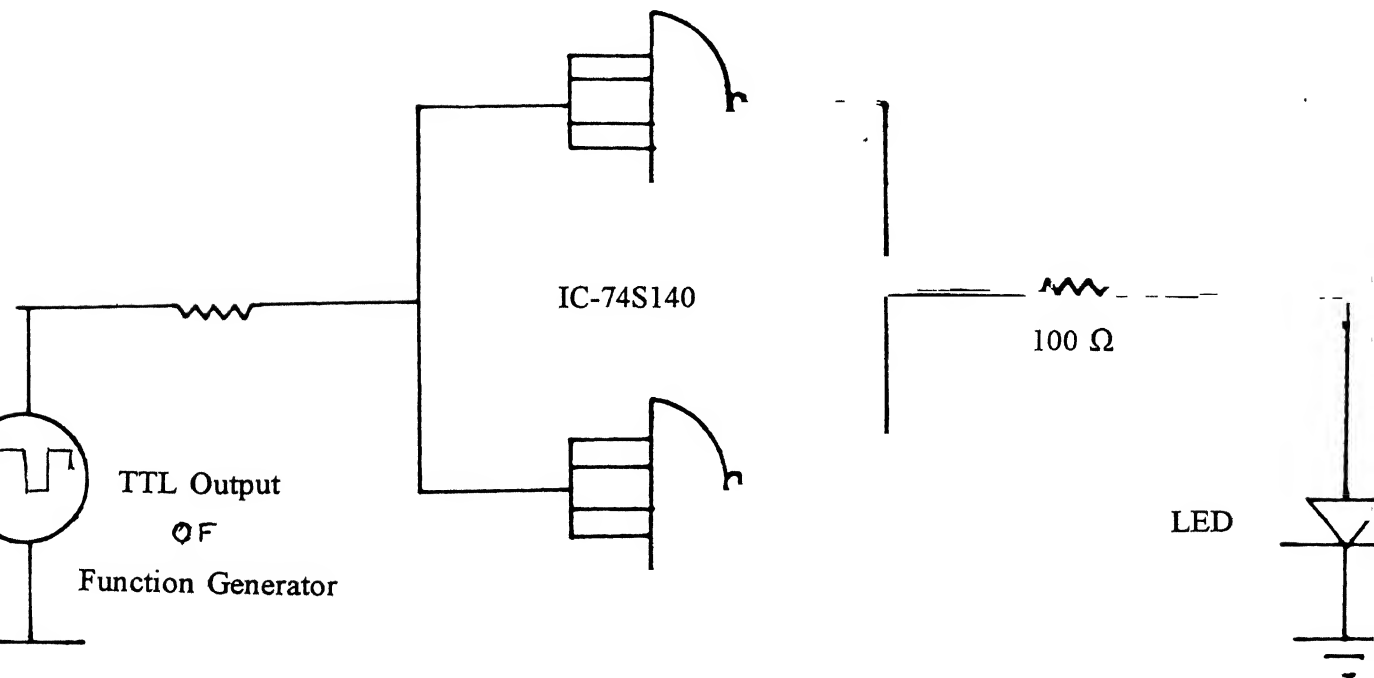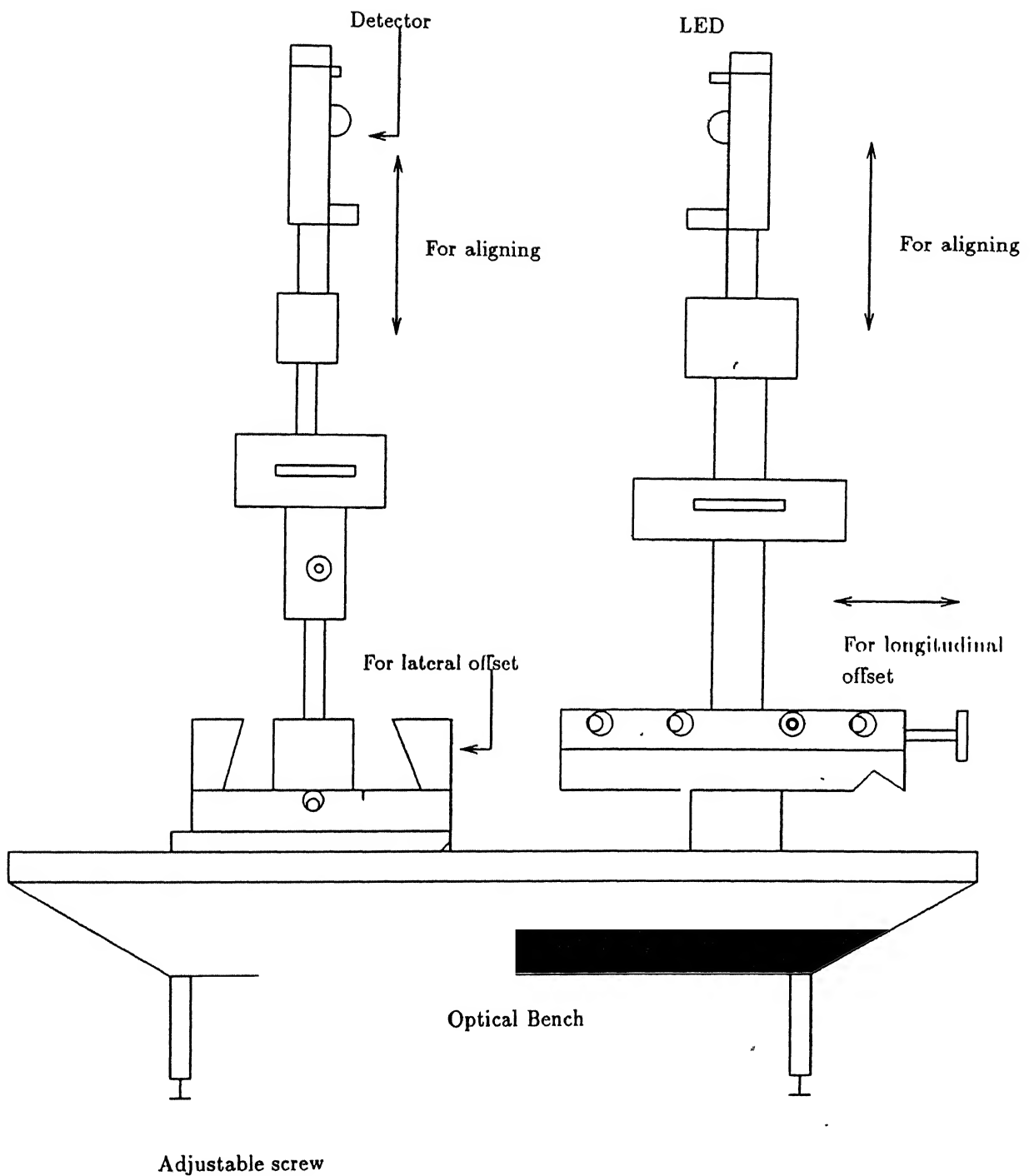Figure 3.2 LED driver circuit to measure the far-field pattern

Detector

LED

For aligning

For aligning

For lateral offset

For longitudinal offset

Optical Bench

Adjustable screw

Figure 3.3: Experimental set-up for measuring the far field pattern of the LED

3.1.1   Driver Circuit for LED

LED driver circuit is shown in fig (3 2). The input signal to the circuit is a square wave of 1 Khz frequency from a function generator. This signal is fed to IC 74S140, 50 Ω line driver, capable of driving upto 60 ma current when two NAND gates are connected in parallel. LED is thus driven by this constant current of approx. 30 ma.

3.1.2   Experimental Setup

Experimental set up for measuring the far field pattern of LED has been shown in fig(3.3). The LED is mounted on a printed circuit board (PCB) and is fixed on the optical bench with a holder The detector is positioned on the optical bench at a distance of 12 cm. from LED. The detector is connected in series with a resistance of 100 KΩ and the output is taken across the resistance The lateral, vertical and rotational knobs are used for source, detector alignments.

3.1.3   Far Field Measurement of LED

In the above experimental set up, the lateral, vertical and rotational knobs are adjusted to get the maximum output from the detector. The LED is now rotated with respect to the detector in both the clockwise and anticlockwise direction, and the detector output voltage is noted down. Angle is read through a protractor arrangement. For radiation pattern in θ-direction, PCB containing LED is rotated The radiation pattern is shown in fig (3.4). For radiation pattern in ϕ-direction, PCB is rotated by 90^0 in vertical plane and same procedure is followed. ϕ-direction radiation pattern is shown in fig. (3.5).

3.1.4   Best Curve Fits for Radiation Pattern

To find out the values of m and n for LED used, polar plots of experimental data were compared with standard polar patterns as shown in fig (3.6) and (3.7). The values of m and n for which best curve fits, are found to be m =80, n =140.

3.1.5 Spot-size Calculation for LED

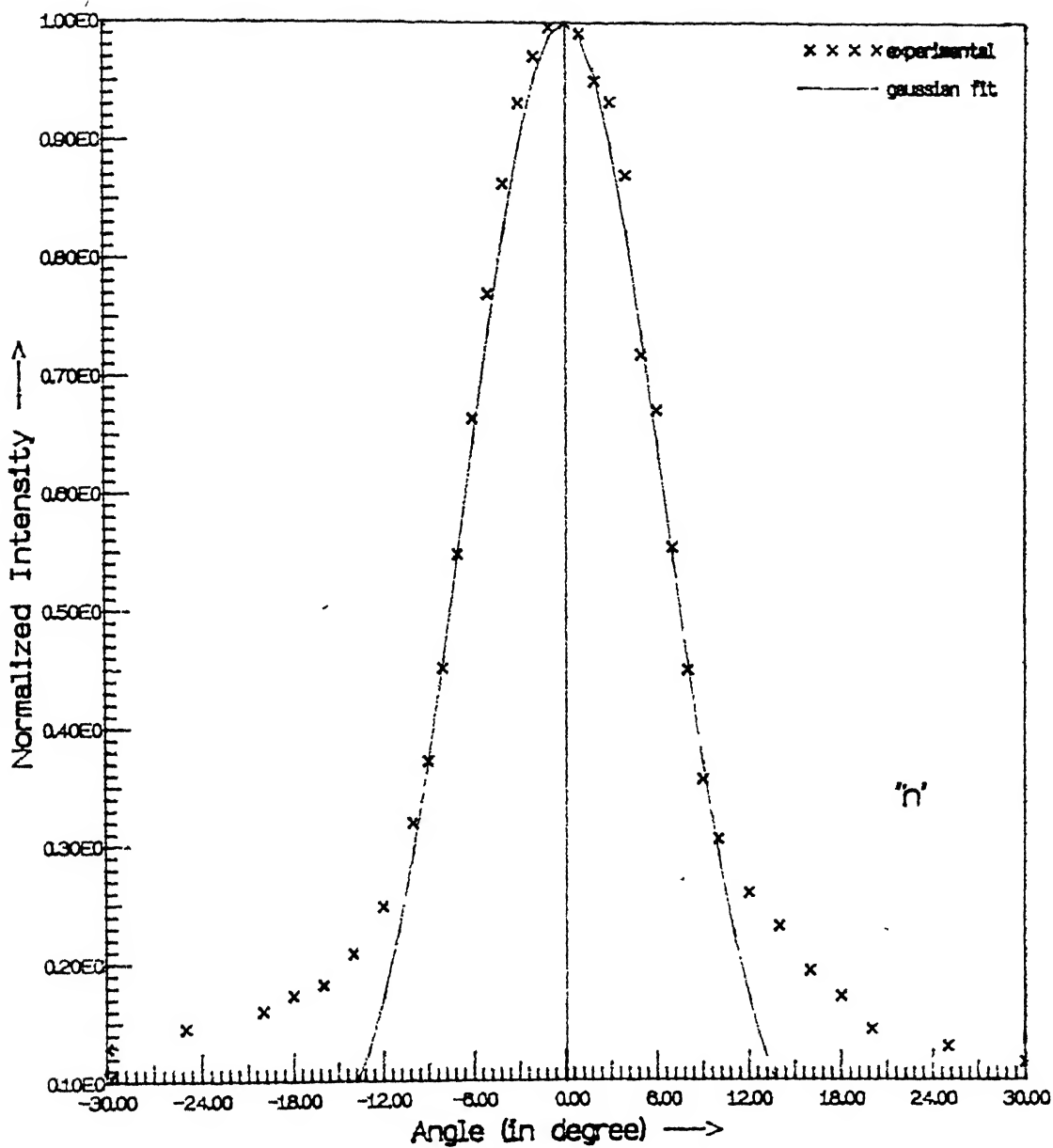We calculate spot-size of LED in both horizontal and vertical direction from source far-

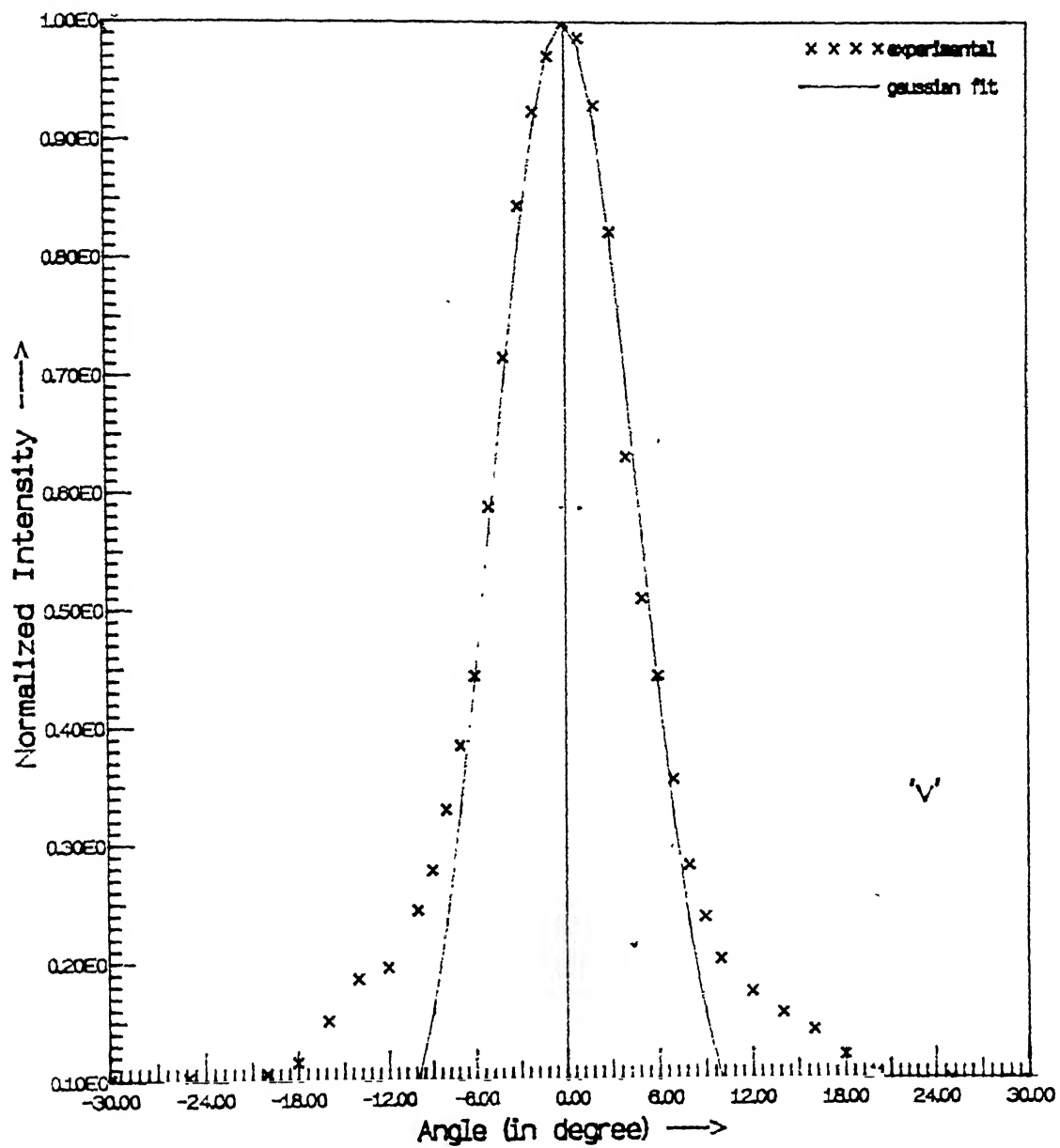Figure 3 4 Measured far-field pattern of LED in horizontal plane and its gaussian fit

Figure 3.5 Measured far-field pattern of LED in vertical plane and its gaussian fit
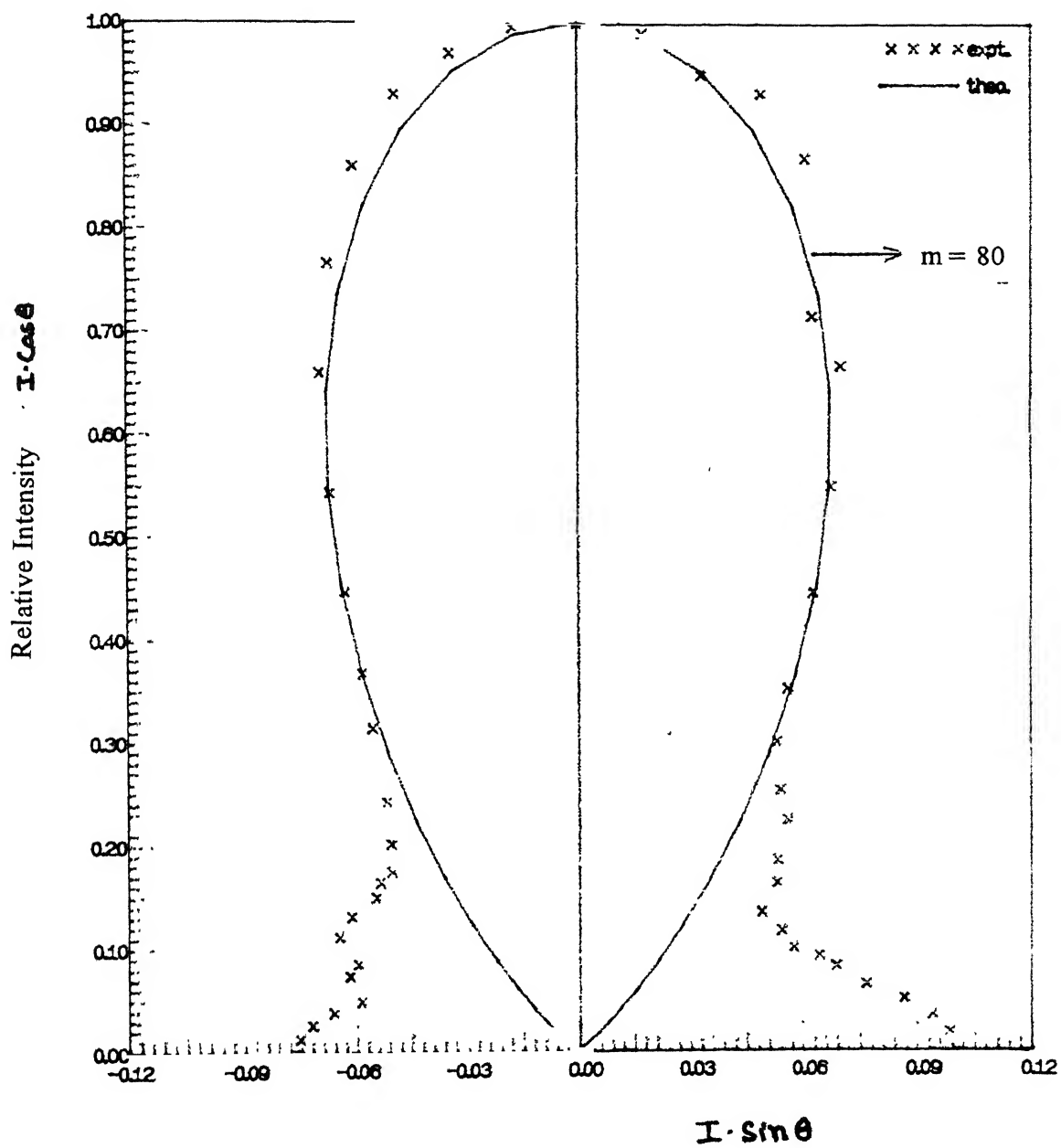
Figure 3.6 Far-field pattern (polar plot) in θ-direction
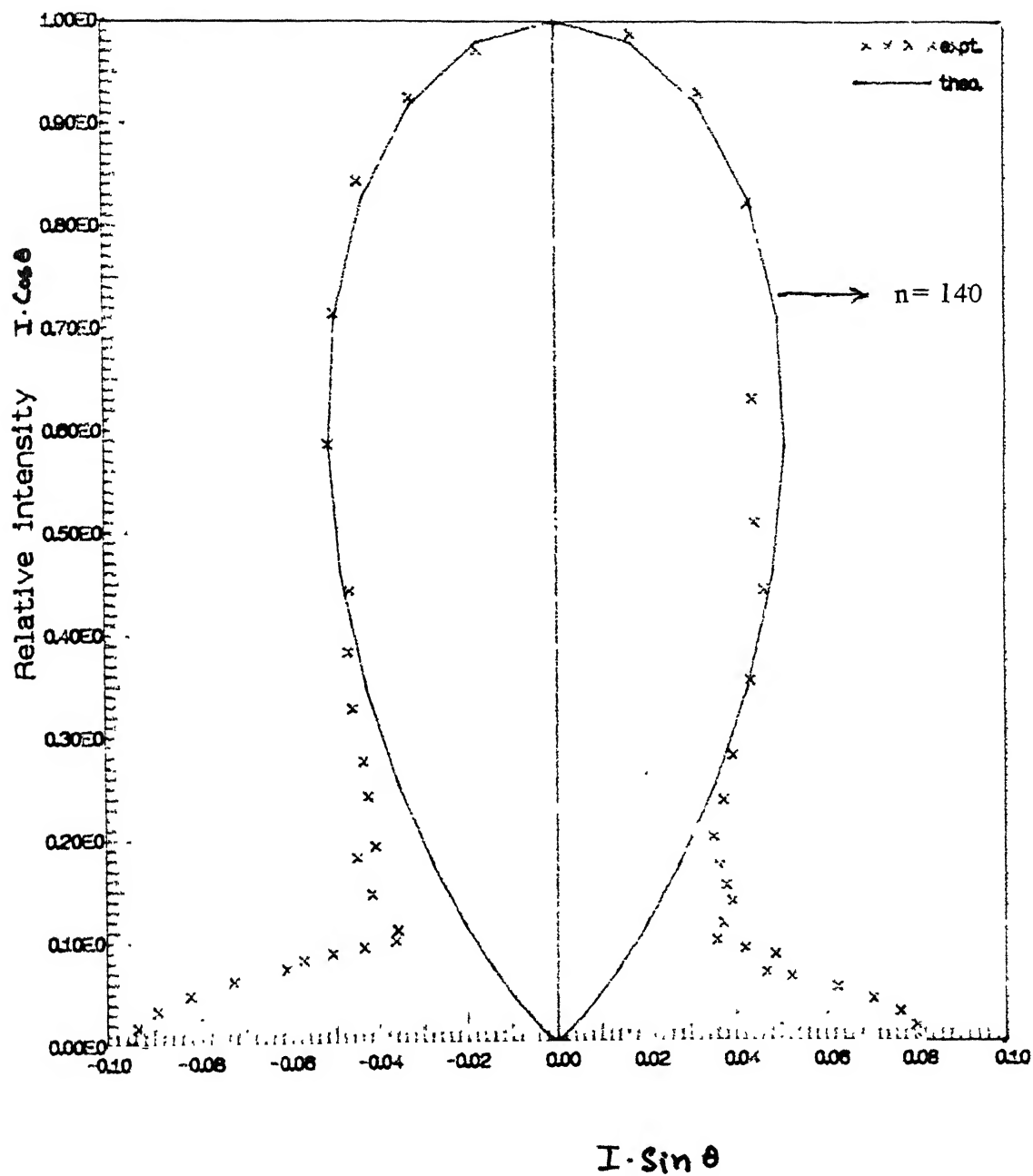
Figure 3 7 Far-field pattern (polar plot) in φ-direction

field patterns and using eqn (2.24) for gaussian beams. This is a crude approximation as the gaussian beam pattern is generally defined for fundamental mode only. In this case the gaussian beam parameters apply to the intensity pattern of the LED. So spot-size is

$$W_0 = \frac{\lambda \sqrt{\ln(2)/2}}{\Pi \tan(\theta_{1/2})} \qquad (3.3)$$

The wavelength of operation is 850 nanometers. $\theta_{1/2}$ is the half of the FWHM angle (full width at half maximum) in a given direction From fig.(3.4) and (3.5), $\theta_{1/2}$ is the half of angle width corresponding to normalized intensity 0.5, and are equal to 7.5^0 and 5.5^0 respectively in horizontal and vertical directions. Spot-sizes to be calculated are as follows,

$$W_{0x} = 1.1814 \ \mu m \qquad , \qquad W_{0y} = 1.6153 \ \mu m$$

Spot sizes of the source are required for the calculation of coupling efficiency from LED to multi-mode fibre, using gaussian beam approximation, discussed in sec.4.4.

3.2 Measurements of Fibre Characteristics

In order to calculate source to fibre coupling efficiencies, some important parameters of optical fibre e.g. numerical aperture, emission half angle etc. must be known with good accuracy Numerical aperture is related to the maximum acceptance angle and is commonly used to describe the light acceptance or gathering capability of a fibre. Emission half angle can also be easily obtained from the far-field radiation pattern of the fibre. These parameters are measured using Universal fibre optic analyzer FOA-1000

3.2.1 Overview of Universal Fibre Optic Analyzer

The universal fibre optic analyzer (FOA-1000) available in the laboratory, is a self-contained precision optical measurement system configured to test complete fibre-optic systems as well as the individual components of a fibre-optic system. It can be used to measure bulk attenuation, pulse dispersion, far and near field angular radiation patterns. From these additional functions such as bandwidth, numerical aperture, index profile etc. can be calculated. This

31

analyzer can also function as optical time domain reflectometer (OTDR) useful for locating fibre breaks, determining fibre length & splice losses.

The system consists of optical components configured in a unique crossover manner, providing compact and versatile measurement system. There are basically two optical paths that share a common crossover point. An optical device placed at this point can change the routing of the optical signals, thereby changing the type of measurement being made. One path runs from the light source to the input (or launch) end of fibre being examined and second path, from output end of the fibre to the detector. A beamsplitter placed at the crossover point converts analyzer in OTDR while reversing the beamsplitter directs light source directly onto detector for pulse signature measurements. Pushing the beamsplitter down switches it out of optical path. The output fibre stage is mounted on a unique rotary stage that allows the fibre to be rotated angularly around its own output end. The exact angular rotation is read out electrically as a voltage.

The analyzer accommodates standard light source (pulsed laser diode), or an semiconductor CW laser and a halogen lamp Any of the sources can be selected with a source-switching mirror. This instrument also has a standard high speed silicon avalanche photodiode (APD) detector and an optional detector. A neutral-density filter wheel is provided to maintain the dynamic range of the optical signals. While a launch numerical aperture wheel is provided to restrict the angle of the cone of light from the source as it enters the fibre. It allows the fibre modes to be controlled at launch.

3.2.2   Experimental Setup

Both the numerical aperture (NA) and emission half angle ($\theta_{1/2}$) can be obtained from the far-field radiation pattern of a fibre. FOA-1000 system uniquely measures the far field pattern of fibre. Optical schematic has been shown in fig 3.8. Here the beamsplitter placed at the

crossover point is switched down so that it goes out of optical path, allowing light from the source to enter the fibre and the detector measuring the light emerging from the fibre output. The fibre has been carefully prepared and perfectly aligned to the optical system. The output end of fibre is swung around its own end, which is optically equivalent to swinging the detector. The exact angular rotation is read out electronically using a digital voltmeter with polarity indicating direction of rotation from normal. One degree corresponds to 100 mV. Now we make a plot of normalized intensity versus angle.

In case the radiation pattern is not symmetrical in one or both axes, fibre should be rotated around both axes. It is easily accomplished by detenting the fibre holder at 90^0 to normal, thereby turning the fibre around its own axis.

3.2.3   Measurement of N.A.

Numerical aperture is directly calculated from the far-field radiation pattern, as obtained above. NA is the sine of the half angle at some relative intensity such as 10% of peak. Far field patterns of plastic and glass fibres have been obtained experimentally and numerical apertures are calculated. From figs. (3.9) and (3.10),

NA for plastic fibre = Sin (21.5^0) = 0.367

NA for glass fibre   = Sin (26.5^0) = 0.431

These measured values of numerical apertures may be higher than the actual ones because of the launches modes not coming to equilibrium for short fibre lengths (upto 50 meters). In our case fibre length is approximately 1.5 meters.

3.2.4   Measurement of Emission Half Angle ($\theta_{1/2}$)

The far field radiation pattern of the fibre determines $\theta_{1/2}$ for fibre. A gaussian fit is obtained for a particular fibre as in fig.(3.9) and (3.10), as given by Botez[2]

$$I (\theta) = \exp \left(-0.69\left(\frac{\theta^2}{\theta_{1/2}^2}\right)\right) \tag{3.4}$$

The value of $\theta_{1/2}$ at which gaussian curve fits the far field pattern of fibre is taken as $\theta_{1/2}$ for that fibre. $\theta_{1/2}$ is also defined as half of FWHM angle, as mentioned earlier.

33

$\theta_{1/2}$ for the plastic fibre is 12^0 .

$\theta_{1/2}$ for the glass fibres is 14^0 .

3.2.5 Calculation of Spot Size and V no. of the Fibres

Since the far field patterns for both the fibres have been approximated as gaussian, we can directly calculate the spot sizes using eqn. (3.3) The wavelength of operation (λ) is 850 nm and $\theta_{1/2}$ has been calculated in the preceding section. Spot sizes are given as follows.

Calculated spot size for plastic fibre = 0.7317 μm

Calculated spot size for glass fibre = 0.6238 μm

V number of fibre is given by eqn.

$$V = \frac{2\pi}{\lambda} \cdot a \cdot NA \qquad (3.5)$$

NA has been obtained experimentally V number for both the fibres are thus easily calculated.

3.2.6 Experimental Results of Fibre

Best gaussian curve fits for both the plastic and glass fibres have been obtained by fitting the experimental far field pattern with a gaussian curve given by eqn.(3.4). See fig. (3.9) and (3.10). Fibre parameters obtained from these patterns have been summarised in table
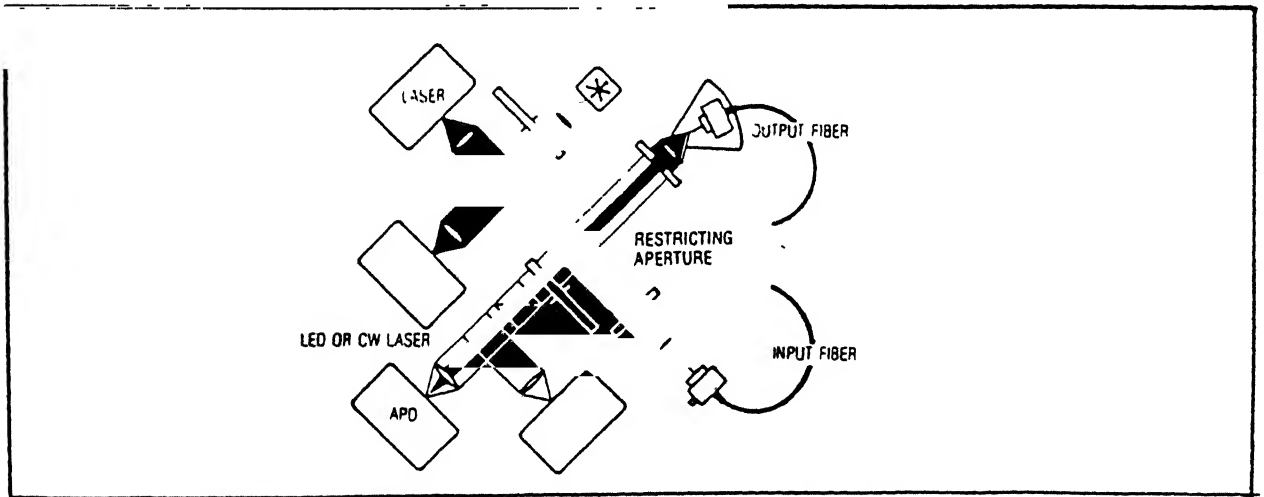

Figure 3.8 Optical schematic of FOA-1000 for the measurement of far-field radiation pattern of the fibre
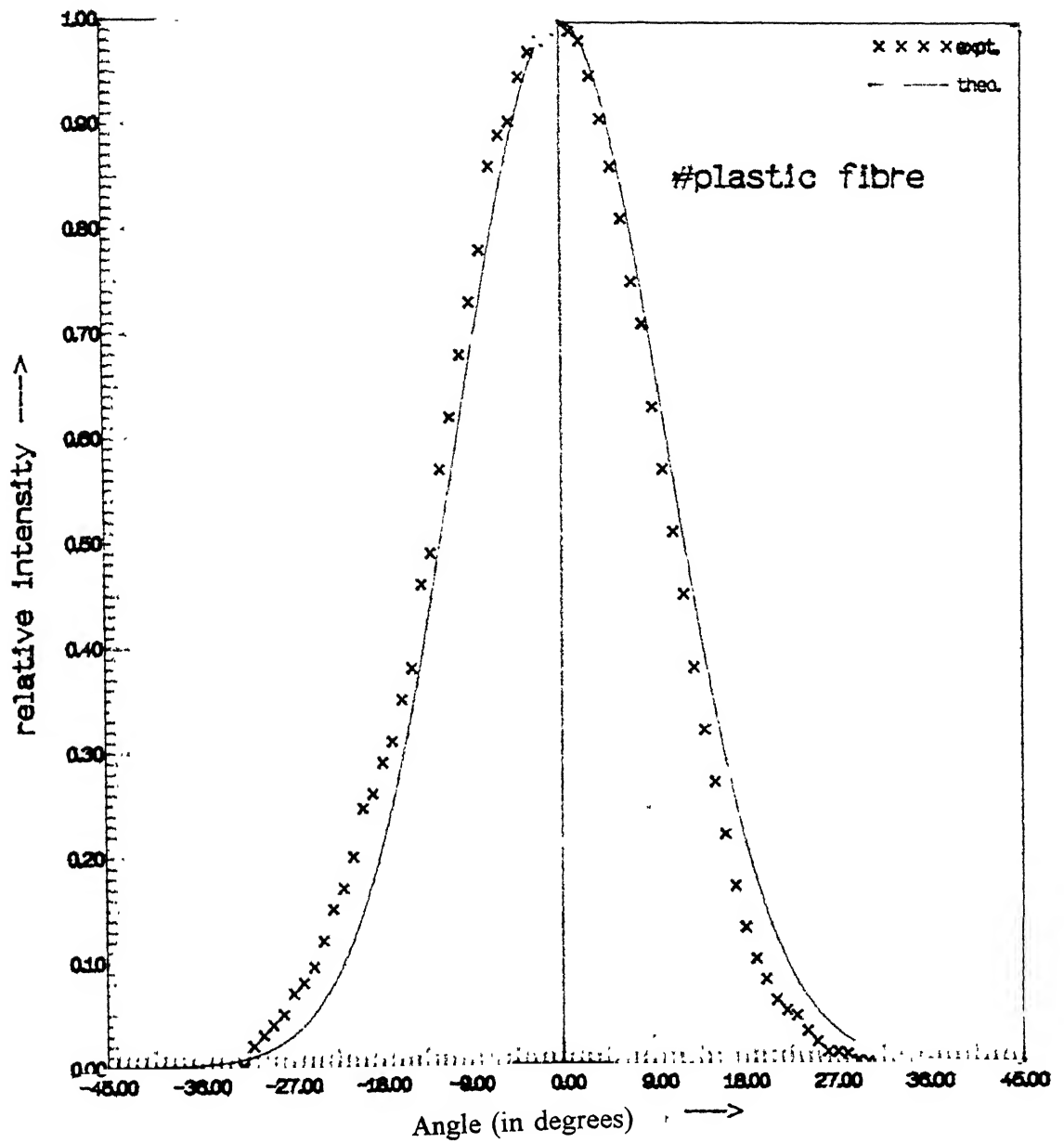
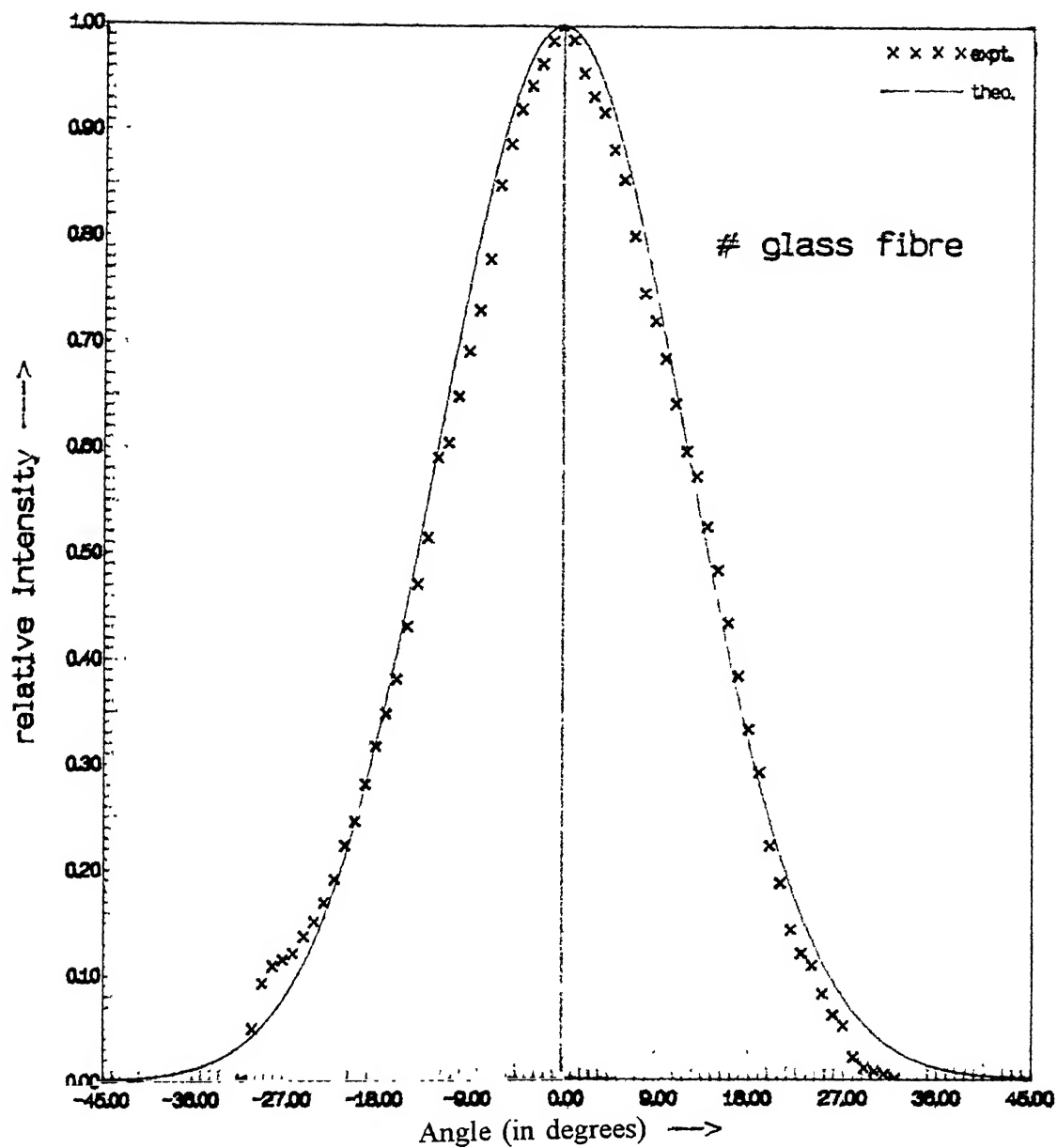Figure 3 9 Measured far-field pattern of plastic fibre and its gaussian fit

Figure 3.10 Measured far-field pattern of glass fibre and its gaussian fit

Table 3.1 Fibre parameters obtained from their far field patterns

Serial no.	Fibre type	Core/Cladding diameter	N.A.	$\theta_{1/2}$	Spot-size
1.	MMF plastic type *Step-index*	1000 µm	0.367	12^0	0.7317 µm
2.	MMF glass type *graded-index*	100/140 µm	0.431	14^0	0.6238 µm

3.3 Experimental Results on Direct and Microlensed Coupling Efficiencies for Various Offsets

Microlenses are formed on the endfaces of plastic and glass fibres in the laboratory. The fibre endfaces are properly prepared. The fibre ends must be flat, perpendicular to the fibre axis and smooth in order not to have light reflected or scattered. Then this smoothed endface is dipped in an optical glue used for splitting fibres. It is cured with ultraviolet rays for about 1 minute and then cooled at room temperature. Since there was no control on the lens parameters, the lenses formed are found to be asymmetrical with arbitrary shape. Two microlenses on plastic fibres (named as microlens-1 and 2) and one microlens on glass fibre (termed as microlens-3) were fabricated and used in our studies.

Coupling efficiencies for these fibres are measured with and without microlenses and compared for longitudinal offset and lateral offset. For longitudinal offset (LED-MMF separation) , the butt coupling efficiency is found to be 48.08% and 49.66% for plastic fibre and 2 respectively and 11.78% for glass fibre After microlens formation on these endfaces coupling efficiency increased to 60.26%, 60.53% and 30.2% respectively. See fig.(3.11), (3.13 and (3.15). For plastic fibres, butt and microlensed coupling efficiencies are approximately th same, except at initial distances, upto 1-2 m.m. The LED outer glass covering has been assume

Figure 3.11   Experimental results: Comparison of direct coupling efficiency with that of microlens-1 on plastic fibre for longitudinal offset

Plastic fibre

Normalized coupling eff. ⟶

(μm)

·△···△·· butt coupling
·◆---◆·· lensed coupling

Figure 3.12 Experimental results: Comparison of direct coupling efficiency with that o microlens-1 on plastic fibre for lateral offset

Figure 3.13   Experimental results: Comparison of direct coupling efficiency with that of microlens-2 on plastic fibre for longitudinal offset
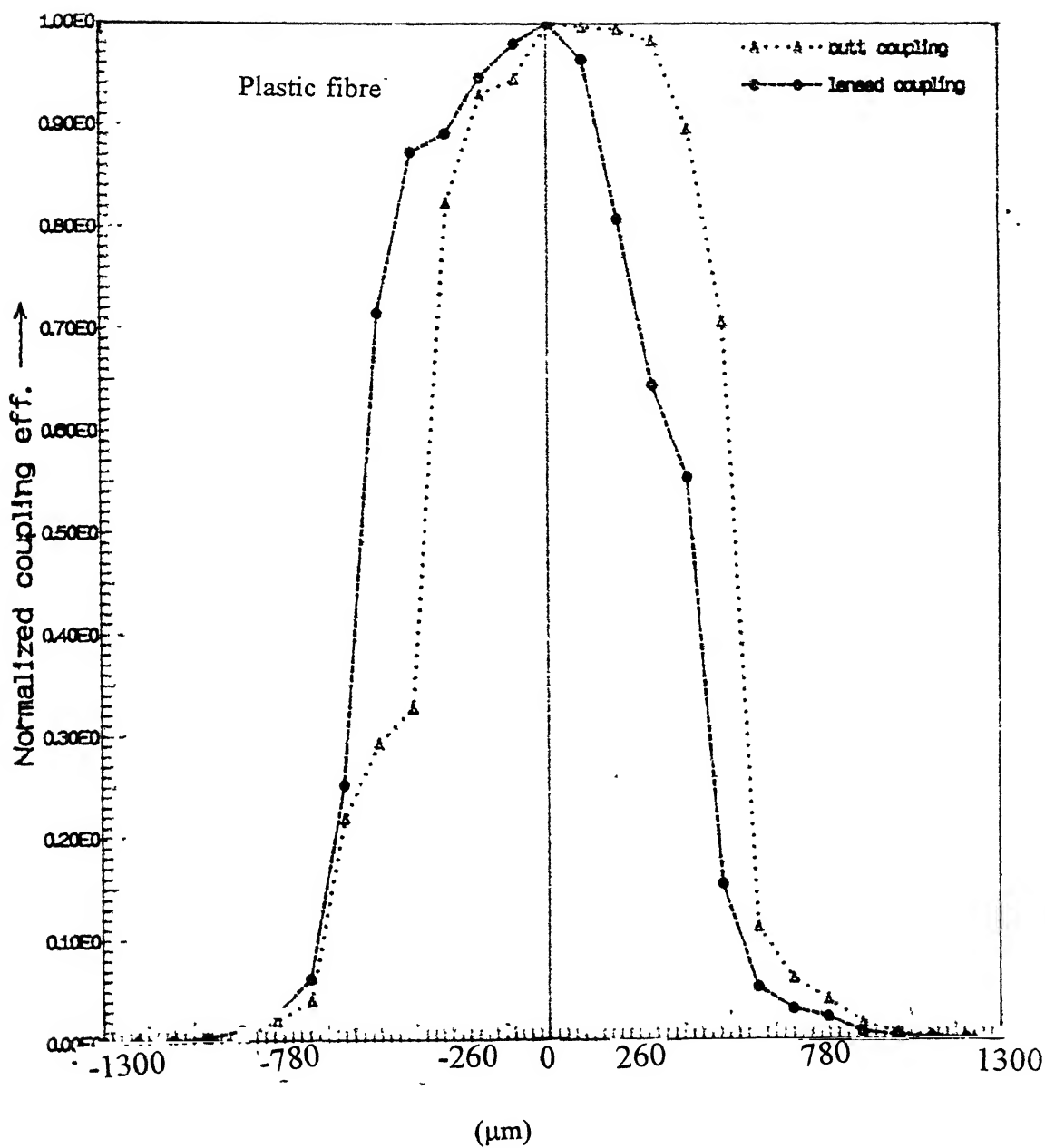
Figure 3.14 Experimental results: Comparison of direct coupling efficiency with that of microlens-2 on plastic fibre for lateral offset
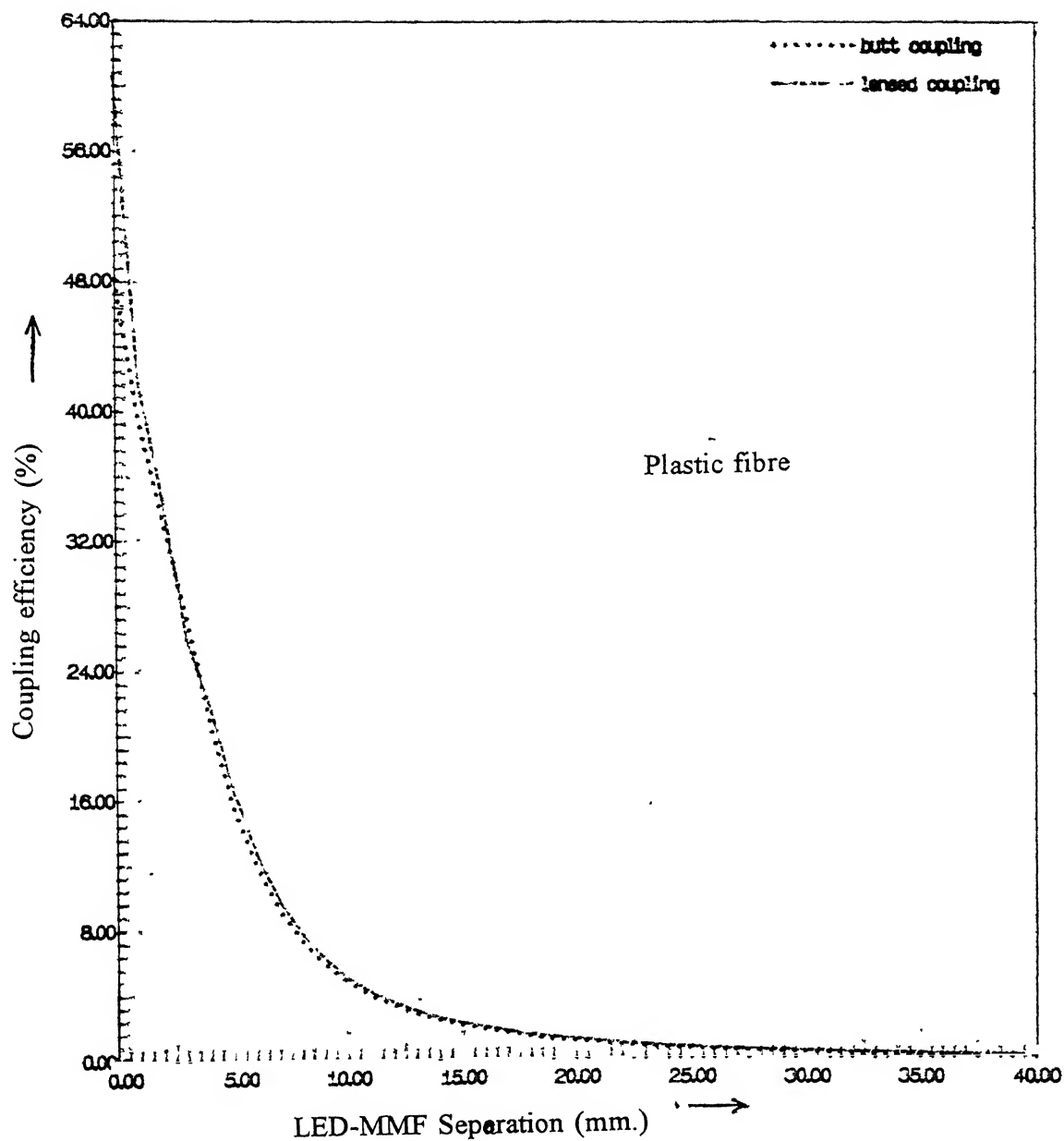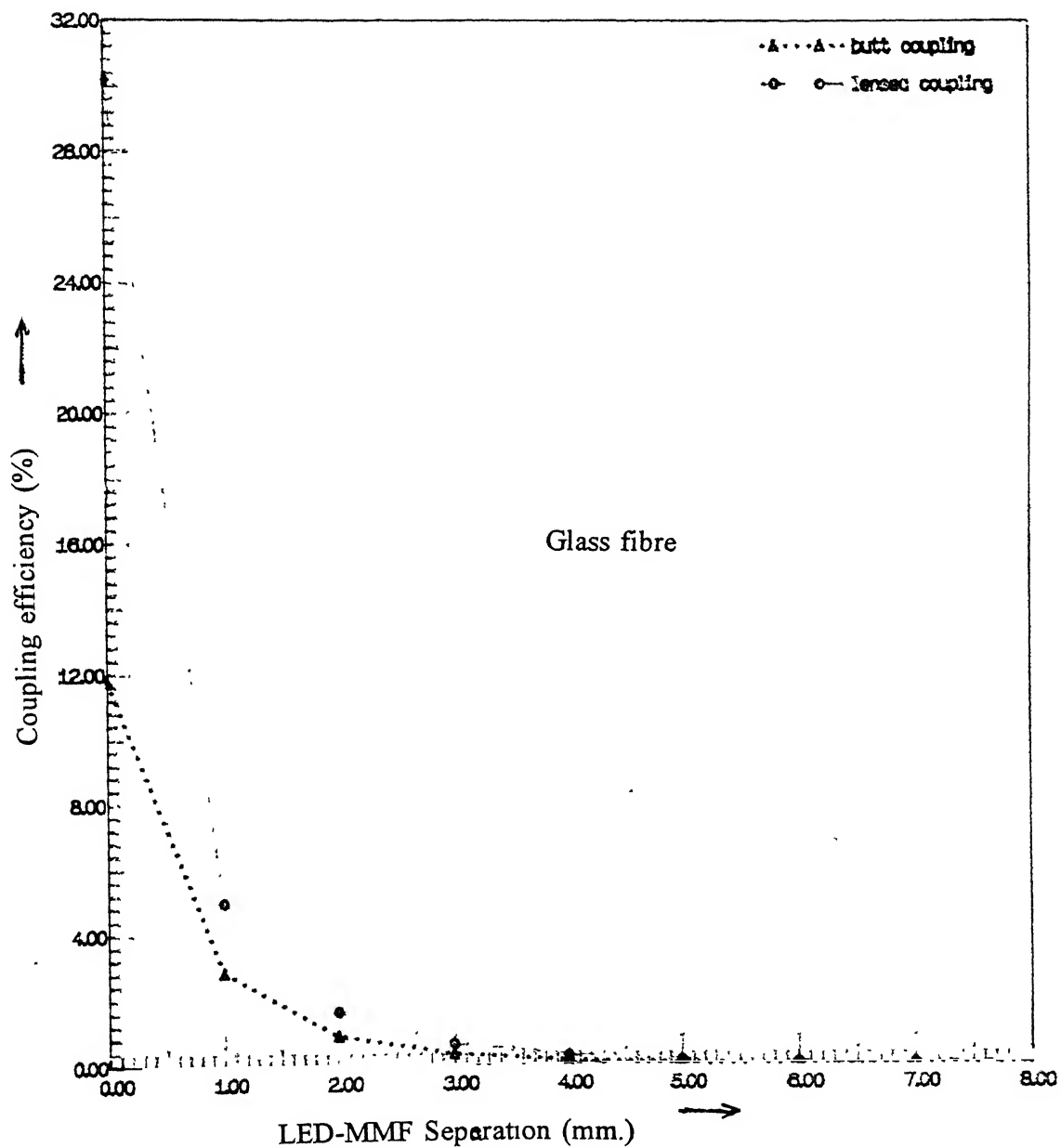
Figure 3.15   Experimental results: Comparison of direct coupling efficiency with that of microlens-3 on glass fibre for longitudinal offset

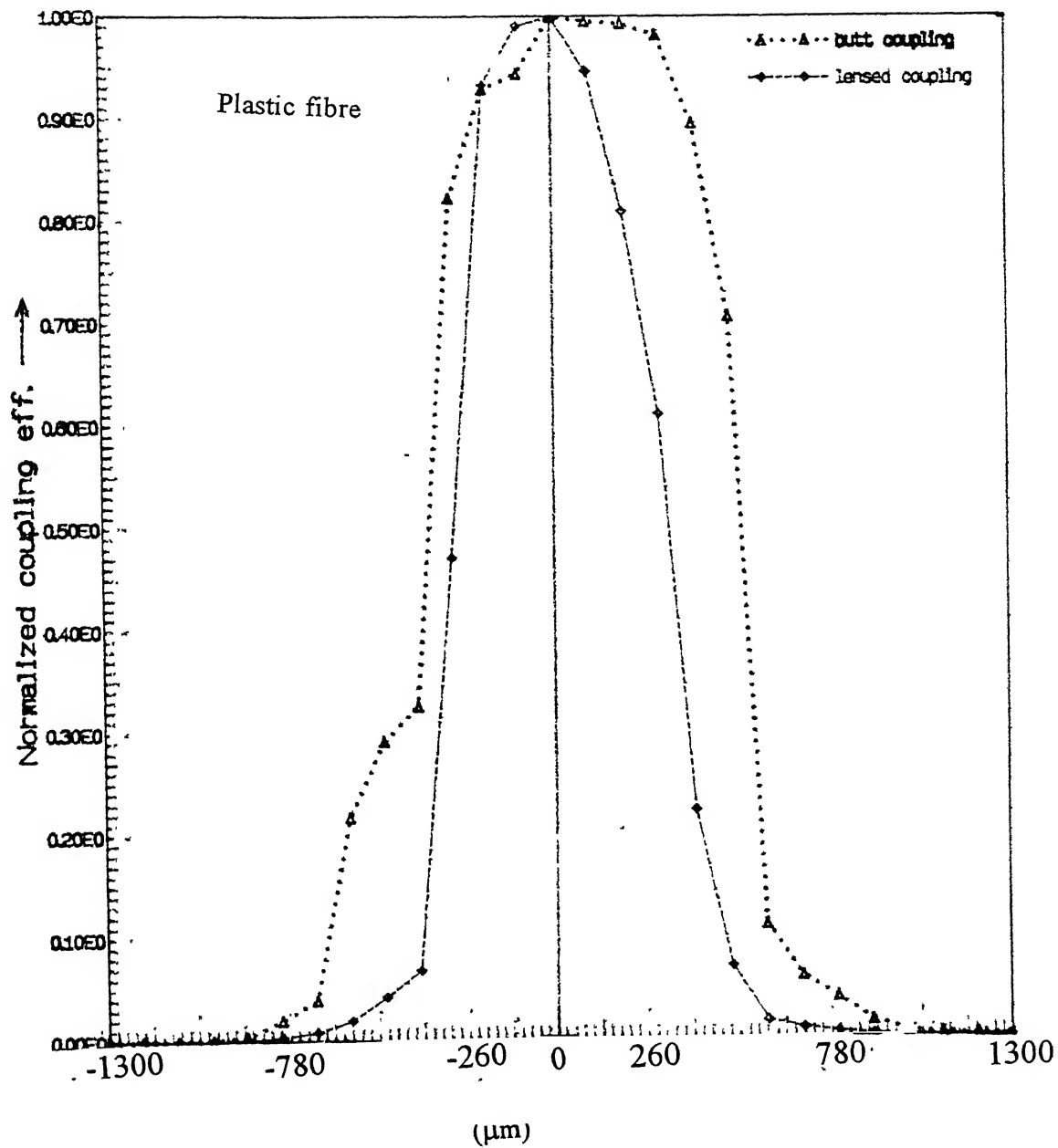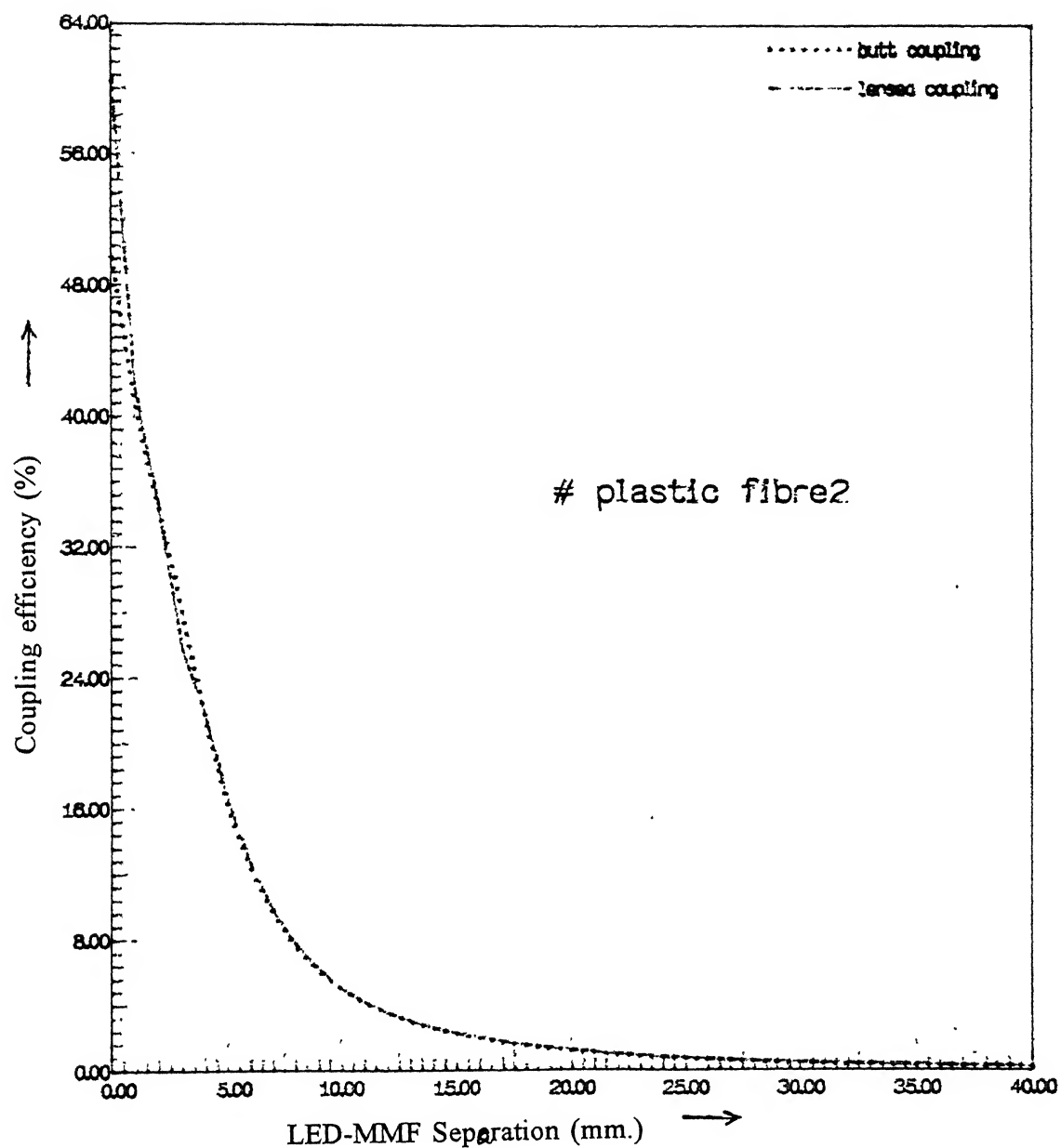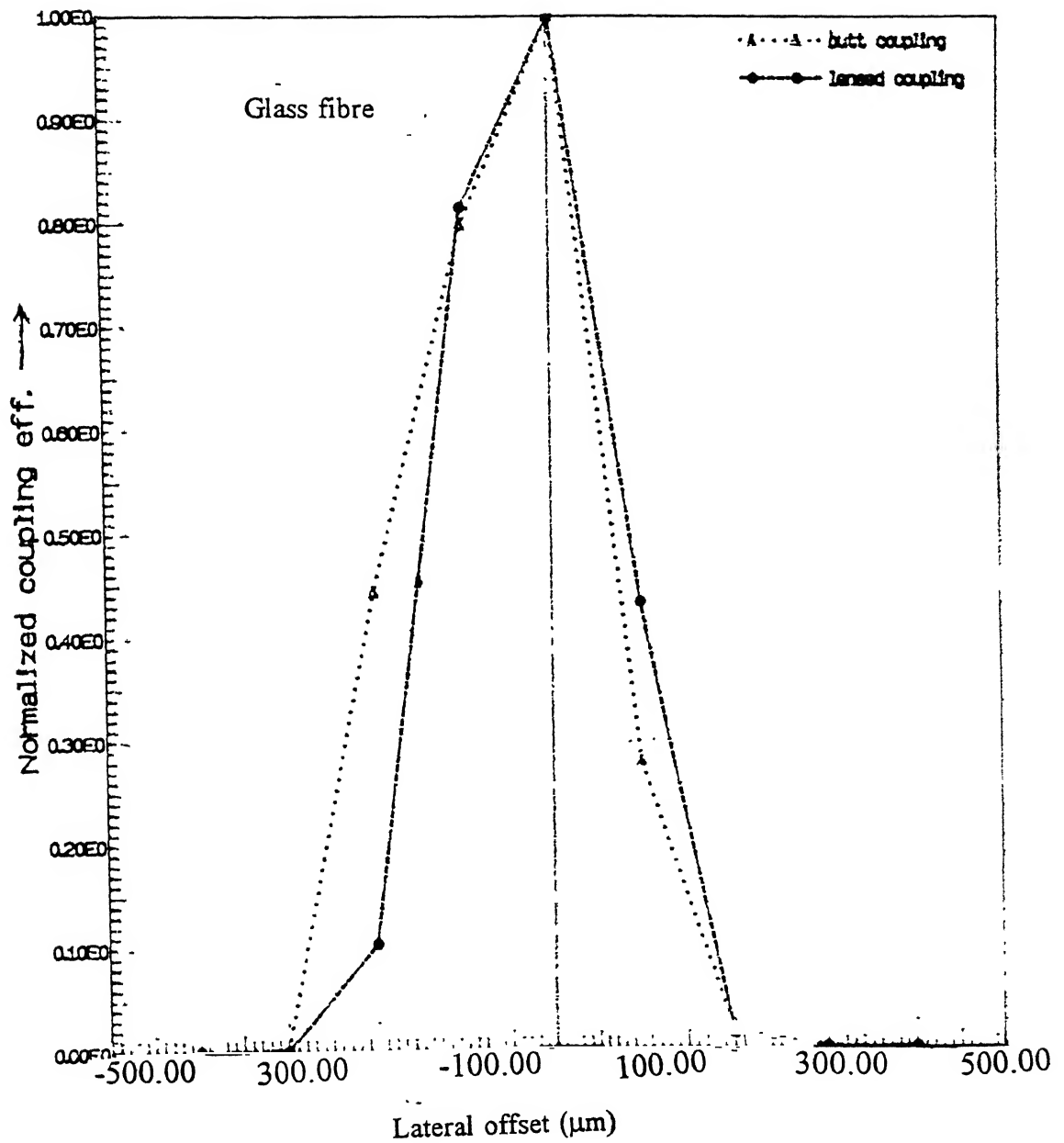Figure 3.16   Experimental results· Comparison of direct coupling efficiency with that of microlens-3 on Glass fibre ፡ for lateral offset

as the reference. For glass fibres, coupling efficiency increased ≈2.5 times after microlens formation.

For lateral offset, the fibres are placed at a point where maximum coupling efficiency is achieved. Lateral offset in the steps of 100 μm are given and plot the variations in normalized coupling efficiency are plotted. See fig. (3 12), (3.14) and (3 16). It is clear that the graphs are not symmetrical. This may be due to the alignment problem of the micropositioners used in the experiment. In the case of microlenses, their asymmetrical shapes might have contributed the asymmetry in the results, in addition to the micropositioner inaccuracies. It is seen that the alignment tolerance decreases with microlens formation on the fibre endfaces.

Summary

Far field radiation pattern of LED source is measured. Best gaussian curve fits and polar plots are obtained. By these we calculate FWHM in both horizontal and vertical directions and hence calculate spot size. Far field patterns of plastic and glass fibres are obtained using Universal fibre optic analyzer, and are found to be gaussian. From these, we calculate numerical apertures, FWHM angles and spot sizes. Improvement of coupling efficiencies for fibres using microlens formation on their endfaces are measured for various offsets.

CHAPTER - 4

LED-MMF Coupling Theory

For optical communication systems using multi-mode fibres (MMFs) with bit rates approximately 100 to 200 Mbps, semiconductor light-emitting diodes (LEDs) are usually the best choice as light sources. LEDs require less complex drive circuitry than laser diodes because no thermal or optical stabilization circuits are needed. They can be fabricated less expensively with higher yields. Since the core size of multimode fibres is much larger than the wavelength of light, the propagation characteristics of light in ideal multimode step-index optical waveguide is most easily seen by simple geometrical approach. So in this chapter, first we will present briefly the ray theory. Then the theories for LED-MMF Coupling are given, using uniform modal power distribution of source, $Cos^m \theta$ and $Cos^n \phi$ radiation patterns of source, and gaussian far field distributions for the LED & MMF. Experimental results of plastic and glass fibres are compared for different coupling theories without any lenses in between (for longitudinal offsets).

4.1   Ray Theory

Ray theory provides a good approximation to the light acceptance and guiding properties of optical fibres when the ratio of fibre radius to the wavelength is large i.e. in multimode fibres where number of guided modes is large. Although mode theory given in sec.2.4.3 is more exact, for MMFs it becomes extremely complex. Ray approach gives more direct physical interpretation of light propagation characteristics in a fibre. There are two types of rays that can propagate in a fibre, viz. meridional rays and skew rays. Meridional rays are confined to the planes, containing the axis of symmetry of fibre, and skew rays not passing through fibre axis Skew rays are not necessary for a general picture of rays propagating in fibre[10]. Meridional rays can be divided into two classes-bound rays that are trapped in core and propagate along the fibre axis, and unbound rays that are refracted out of the fibre core. See fig. 4.1. The light rays enters the fibre core from a medium of refractive index n_0 at an angle θ_0 with respect to the fibre axis and strikes the core-cladding interface at normal angle ϕ. From Snell's law, the minimum angle that supports total

internal reflection is given by,

$$\sin \Phi_c = \frac{n_2}{n_1} \qquad (4.1)$$

Where n_1 and n_2 are core and cladding refractive indices respectively. If $\phi > \phi_c$, total internal reflection takes place at the core-cladding interface and gets propagated along fibre core. If $\phi > \phi_c$, rays will refract out of core and will be lost in cladding.

Figure 4.1 Meridional ray optics representation and the acceptance angle in an ideal step-index optical waveguide

Maximum entrance angle is given by

$$n_0 \sin \theta_{0,max} = n_1 \sin (90 - \Phi_c) = \sqrt{n_1^2 - n_2^2} \qquad (4.2)$$

The fibre accepts only those rays contained within a cone whose maximum angle is $\theta_{0,max}$ i.e. rays

38

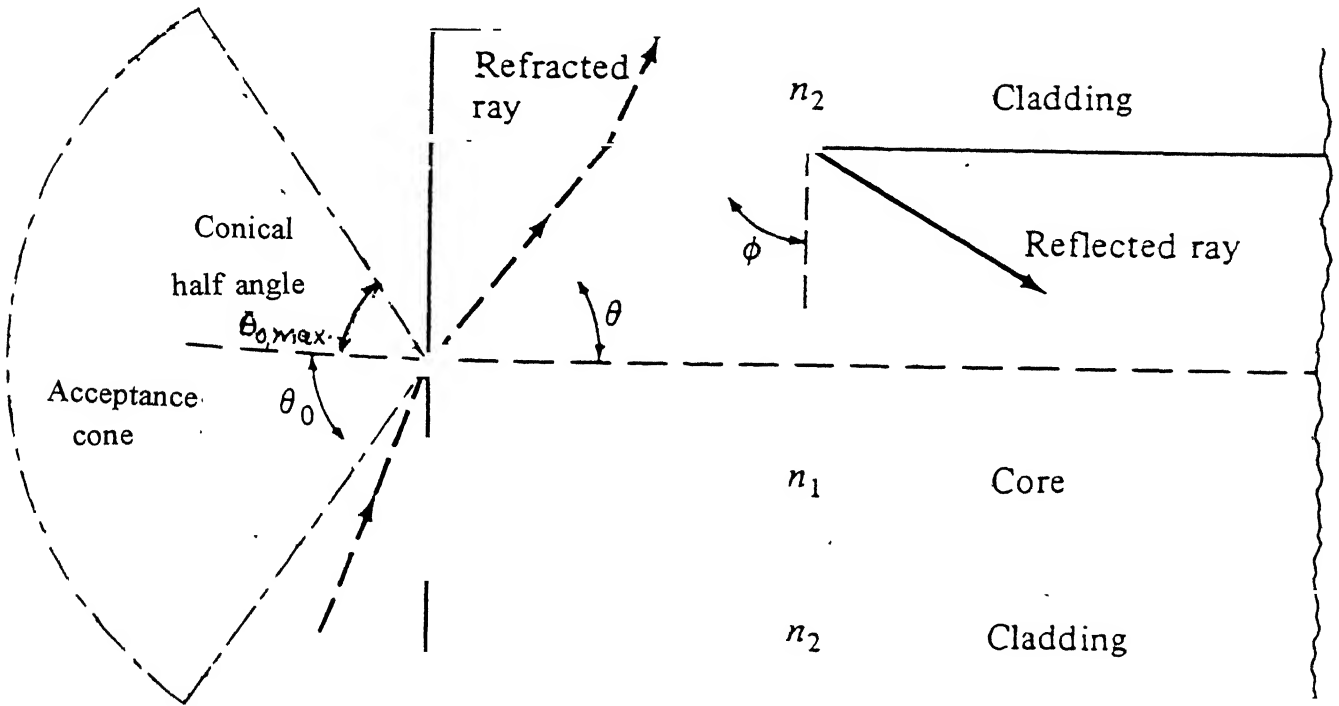

Figure 4.1 Meridional ray optics representation and the acceptance angle in an ideal step-index optical waveguide

Maximum entrance angle is given by

$$n_0 \sin \theta_{0,max} = n_1 \sin (90 - \Phi_c) = \sqrt{n_1^2 - n_2^2} \qquad (4.2)$$

The fibre accepts only those rays contained within a cone whose maximum angle is $\theta_{0,max}$ i.e. rays

38

4.2   Coupling Theory Assuming Uniform Modal Power Distribution

This is a simple theory in which we assume that the rectangular light emitting region of an LED results in elliptical, divergent beam profile and that the power is uniformly distributed in the elliptic cross-section See fig (4.2). The power coupled into the fibre is given by the overlapping area of emitted diverged beam and the fibre cross section. This model has also been reffered as Model-1 in our theory

Also we approximate the elliptic beam to be constituted of two circularly symmetric independent component, perpendicular to each other The total coupling efficiency is thus given by the geometric mean of the two coupling efficiencies of the independent components. i.e.

$$\eta = (\eta_{\theta\perp} \cdot \eta_{\theta\parallel})^{1/2} \tag{4.5}$$

Let a and b be half of the major and minor axes of the ellipse, and R_f be the radius of MMF. For one independent circularly symmetric component, [see fig (4.3)]

$$R_1 = d \tan \theta \tag{4.6}$$

where d is the separation between source and fibre, and θ is the angle of the emitted cone from source Since fibre will accept rays having angle $< \theta_{0,max}$, we get

$$R_{1,max} = d \tan \theta_{0,max} \tag{4.7}$$

where $\theta_{0,max}$ is given by eqn.(4.3).
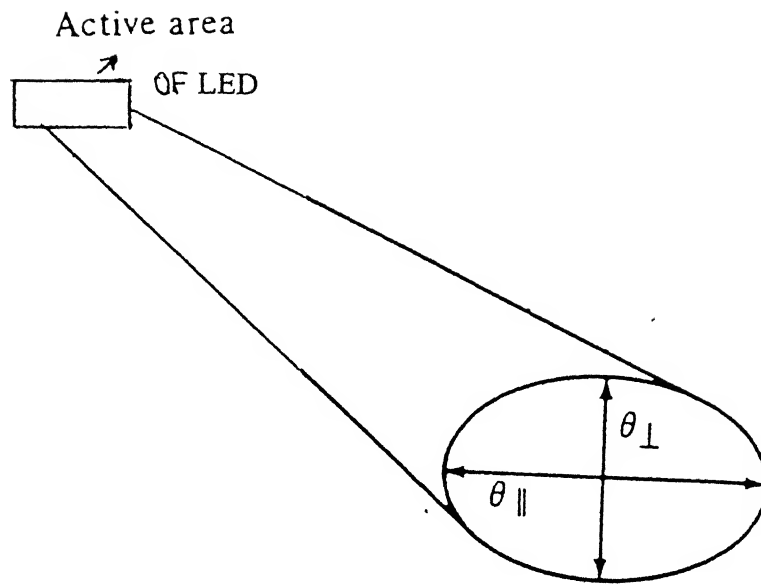
39 (b)

Figure 4.2 Elliptical, divergent beam profile of LED
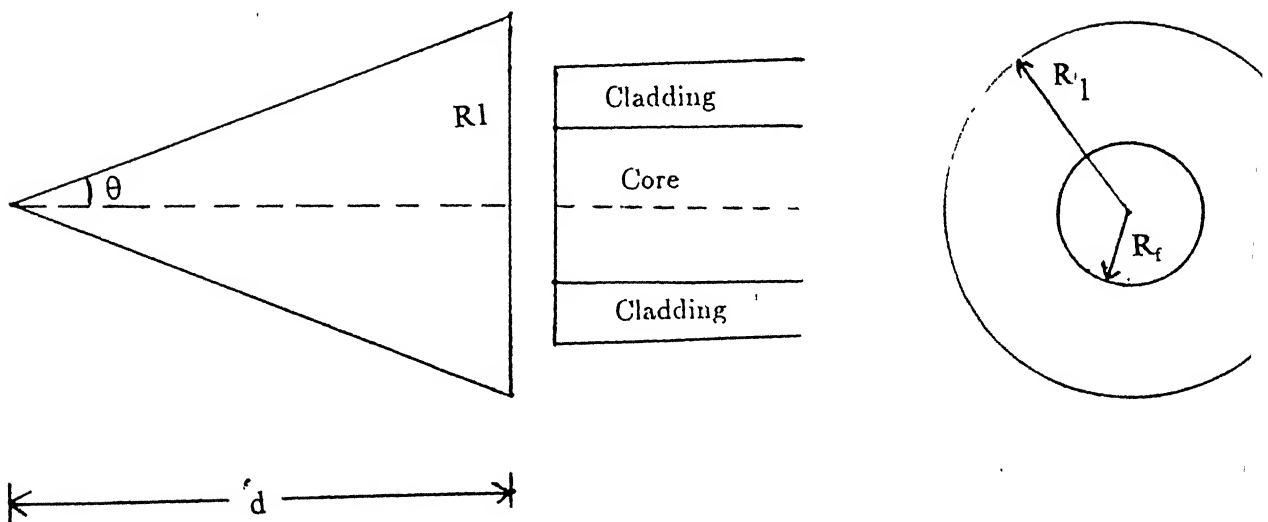

Figure 4.3 Source-fibre coupling for longitudinal offset, assuming uniform model power
distribution

$$R_{1,max} = d \tan \theta_{0,max} \qquad\qquad (4.7)$$

Now coupling efficiency is obtained by calculating the fraction of the power intercepted by fibre. As shown in fig 4.3 , the two regions of interest are

(1.) $R_{1,max} \leq R_f$, whole power is intercepted by the fibre, hence coupling efficiency, $\qquad \eta = 1.0$.

(ii.) $R_{1,max} > R_f$; η is the ratio of area of fibre to that of the beam.

$$\eta = \frac{\pi R_f^2}{\pi R_{1,max}^2} = \frac{R_f^2}{d^2 \tan^2\theta_{0,max}} \qquad\qquad (4.8)$$

Similar expressions can be written for the another component.

Also $R_{1,max} \leq R_f \Rightarrow d \leq R_f / \tan \theta_{0,max}$.

So total coupling efficiency is given by, using eqn.(4.5), (4.7) and (4.8)

$$1) \quad for \quad d \leq \frac{R_f}{\tan \theta_{0,max}} \qquad , \quad \eta = 1.0 \qquad\qquad (4.9)$$

$$2) \quad for \quad d > \frac{R_f}{\tan \theta_{0,max}} \qquad , \quad \eta = \frac{R_f^2}{d^2 \tan^2\theta_{0,max}} \qquad\qquad (4.10)$$

Using the above expressions given, LED-MMF coupling efficiency (for both plastic and glass fibres) is calculated for various longitudinal separation d. These theoretical results have been compared with the experimental results and shown in fig(4.4) and (4.5). Detailed discussions on these are given in sec. 4.5 .

Coupling losses strongly depend on input power distribution. Uniform distribution causes the highest sensitivity to mismatches[15] . So results should indicate the worst case for practical fibre systems

4.3 Coupling Theory Assuming Cos^m θ and Cos^n φ Distributions of Source

In this theory, the far-field patterns of LED have been assumed to vary approximately as Cos^m θ in perpendicular direction and as Cos^n φ in the parallel direction to the junction plane. It is also assumed that the cross-sectional area of the radiation pattern at the entrance plane of the fibre is less than or equal to fibre bundle area. This analysis also includes only bound or trapped rays, propagating in the direction of the waveguide axis, and leaky modes
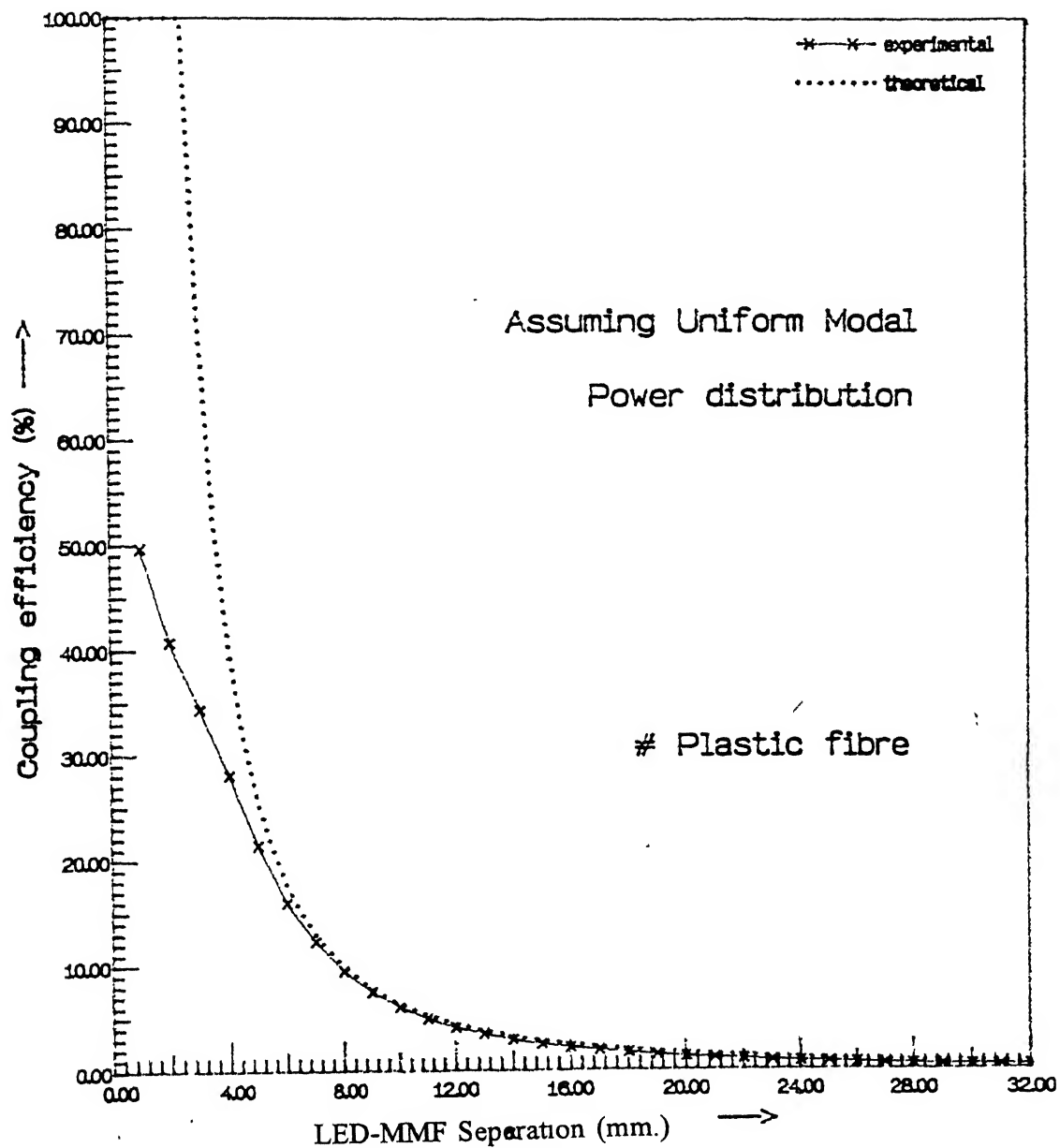
Figure 4.4, Comparison of measured coupling efficiency with the calculated one for longitudinal offset for plastic fibre (Model-1)
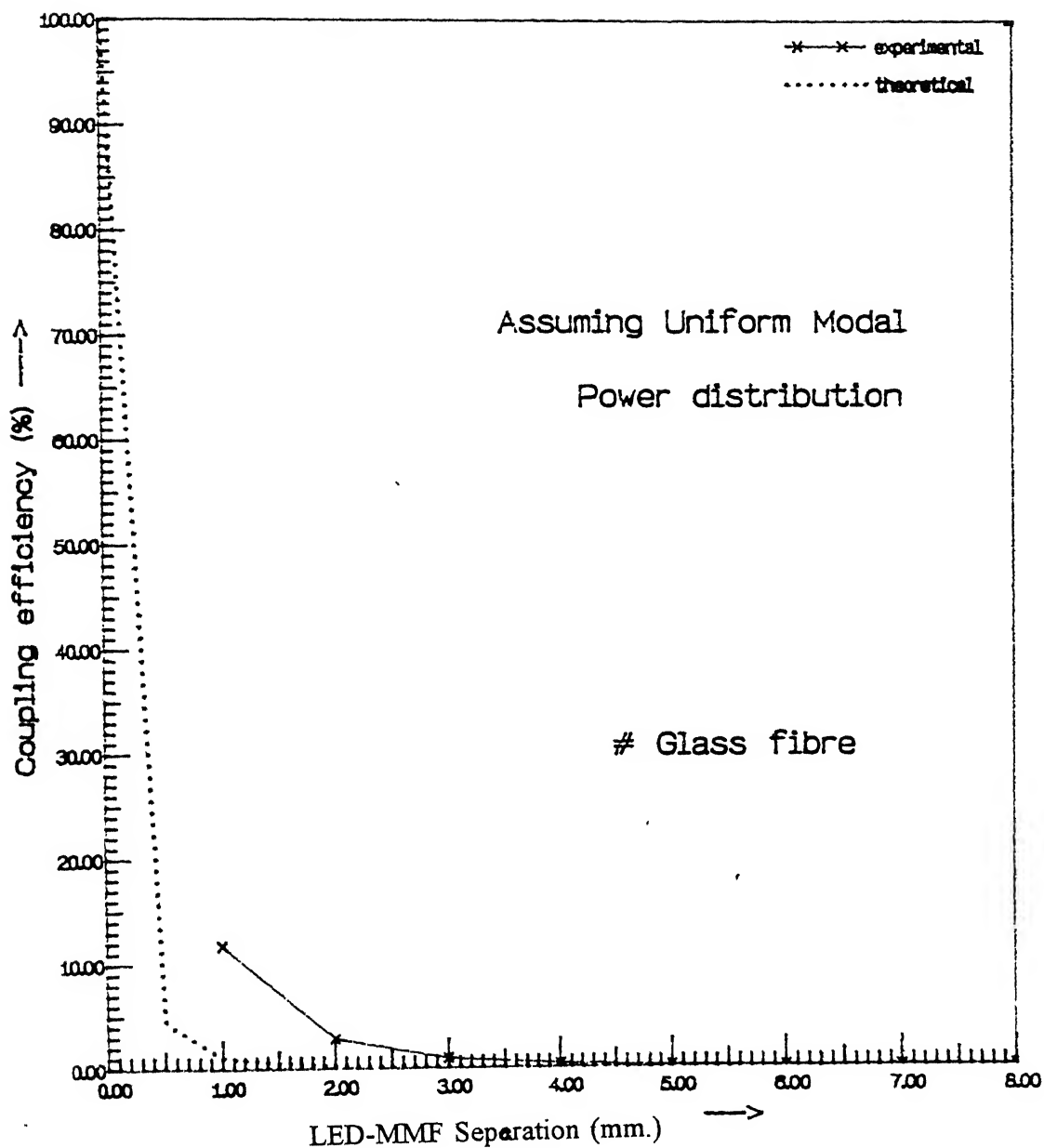
Figure 4.5 Comparison of measured coupling efficiency with the calculated one for longitudinal offset for glass fibre (Model-1)

are neglected. This model has also been reffered as (Model-2) in our theory

If optoelectronic source is directly butted against the fibre, the power coupled into the fibre is given by[1]

$$P_c = 2\pi A_{source} \ f_P \int_0^{\theta_0} B(\theta) \ \sin\theta \ d\theta \qquad (4.11)$$

where $B(\theta)$ is the angular distribution of source brightness, A_{source} is the source emitting area and f_P is the packing fraction. For single fibre, f_P is unity.

For our case, angular distribution of the LED-source brightness has been expressed as $B(\theta) = B(0). \ Cos^m \ \theta$ and $B(\phi) = B(0). \ Cos^n \ \phi$ in θ and ϕ direction.

Similar to sec.(4.2), we will calculate coupling efficiencies using these radiation patterns independently and find geometric mean to get the total coupling efficiency. So in the θ-direction, putting $B(\theta) = Cos^m \ \theta$ in eqn.(4.11), we get

$$P_{\eta 1} = 2\pi A_{source} \int_0^{\theta_1} B(0). \ \cos^m \theta . \ \sin \theta . \ d\theta$$

$$= P_0 \int_0^{\theta_1} \cos^m \theta . \ \sin \theta . \ d\theta \qquad (4.12)$$

P_0 will be a constant quantity, given by

$$P_0 = 2\pi A_{source} . \ B(0) \qquad (4.13)$$

The total optical output power emitted from the source into the full hemisphere is given by

$$P_{tot} = 2\pi A_{source} \int_0^{\frac{\pi}{2}} B(0) . \ \cos^m \theta . \ \sin \theta . \ d\theta$$

41

putting $\theta_1 = \pi/2$ So

$$= P_0 \cdot \int_0^{\frac{\pi}{2}} \cos^m \theta \cdot \sin \theta \cdot d\theta$$

$$= P_0 \cdot \int_0^1 t^m \cdot dt$$

$$= \frac{P_0}{m + 1} \qquad\qquad (4.14)$$

so from eqn.(4.12) and (4.14), coupling efficiency will be

$$\eta_1 = \frac{P_{c1}}{P_{tot}} = (m+1) \int_0^{\theta_1} \cos^m \theta \cdot \sin \theta \cdot d\theta \qquad (4.15)$$

Similarly for $B(\phi) = B(0) \cdot \cos^n \phi$, coupling efficiency will be

$$\eta_2 = \frac{P_{c2}}{P_{tot}} = (n + 1) \int_0^{\Phi_1} \cos^n \Phi \cdot \sin \Phi \cdot d\Phi \qquad (4.16)$$

First we find θ_1 and ϕ_1. Consider fig(4.6) in θ-plane, we have

$$R_f = d \cdot \tan \theta_0 \quad \longrightarrow \quad d = \frac{R_f}{\tan \theta_0} \qquad (4.17)$$

where d is the longitudinal seperation between LED and MMF, and R_f is fibre radius.
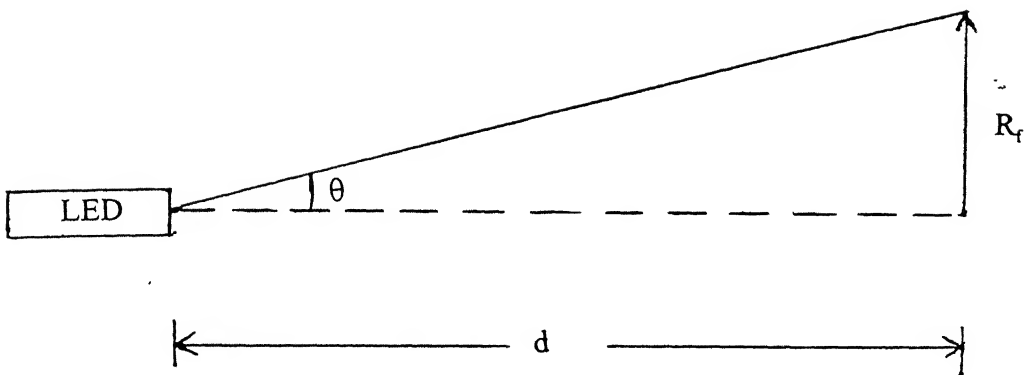
Figure 4.6 Source-fibre coupling for longitudinal offset, assuming $\cos^m \theta$ distribution of source
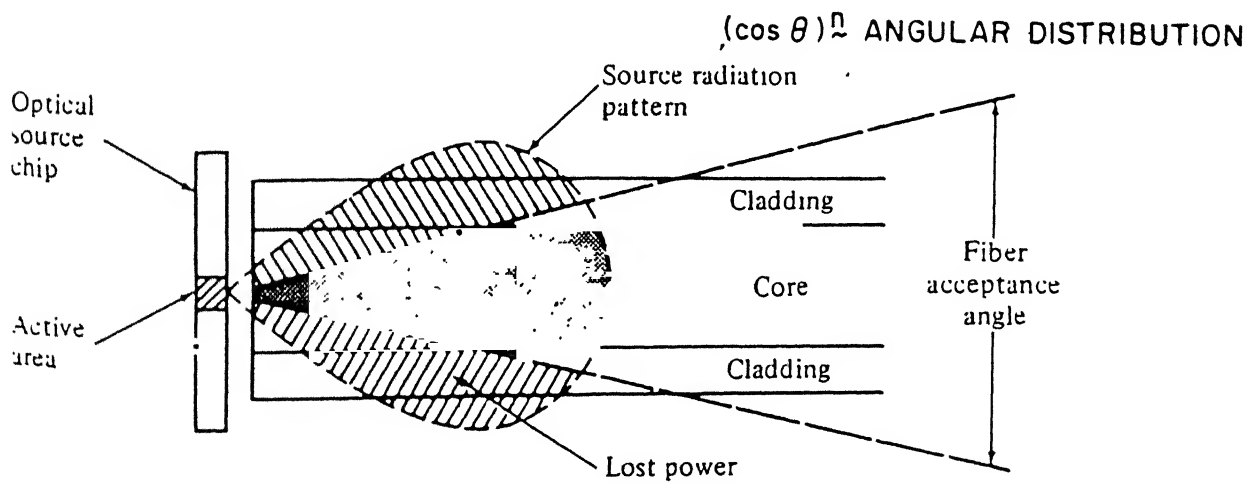

Figure 4.7 Optical source coupled to an optical fibre. (Light outside the acceptance angle is lost.)

If $\theta_0 > \theta_{0,max}$, we see that only rays having acceptance angle less than $\theta_{0,max}$ will be guided along the fibre due to total internal reflection. See fig(4.7). So θ_1 limit will have to be defined in two regions, i.e

$$If \quad d \leq \frac{R_f}{\tan \theta_{0,max}} \qquad \theta_1 = \theta_{0,max} \qquad (4.18)$$

otherwise,

$$If \quad d > \frac{R_f}{\tan \theta_{0,max}} \qquad \theta_1 = \tan^{-1}\left(\frac{R_f}{d}\right) \qquad (4.19)$$

Applying these limits for θ and ϕ cases, we get

$$1) \quad If \quad d \leq \frac{R_f}{\tan \theta_{0,max}} \qquad \theta_1 = \Phi_1 = \theta_{0,max} \qquad (4.20)$$

$$2) \quad If \quad d > \frac{R_f}{\tan \theta_{0,max}} \qquad \theta_1 = \Phi_1 = \tan^{-1}\left(\frac{R_f}{d}\right) \quad (4.21)$$

Using eqn.(4.5), (4.15) and (4.16), the coupling efficiency is given by,

$$\eta = \left[(m+1)(n+1) \int_0^{\theta_1} \cos^m \theta \cdot \sin \theta \cdot d\theta \cdot \int_0^{\Phi_1} \cos^m \Phi \cdot \sin \Phi \cdot d\Phi \right]^{1/2}$$

$$(4.22)$$

where the integeration limits θ_1 and ϕ_1 are given by eqn.(4.20) & (4.21)

Theoretical LED-MMF Coupling efficiency for various longitudinal seperations d is obtained through a software program. These results have been compared with experimental results in fig.(4.8) & fig.(4.9) and are in good agreement especially for glass fibres. Detailed comparison has been presented later in this chapter.

4.4 Coupling Theory Using Gaussian Far-field Patterns for Source and Fibre

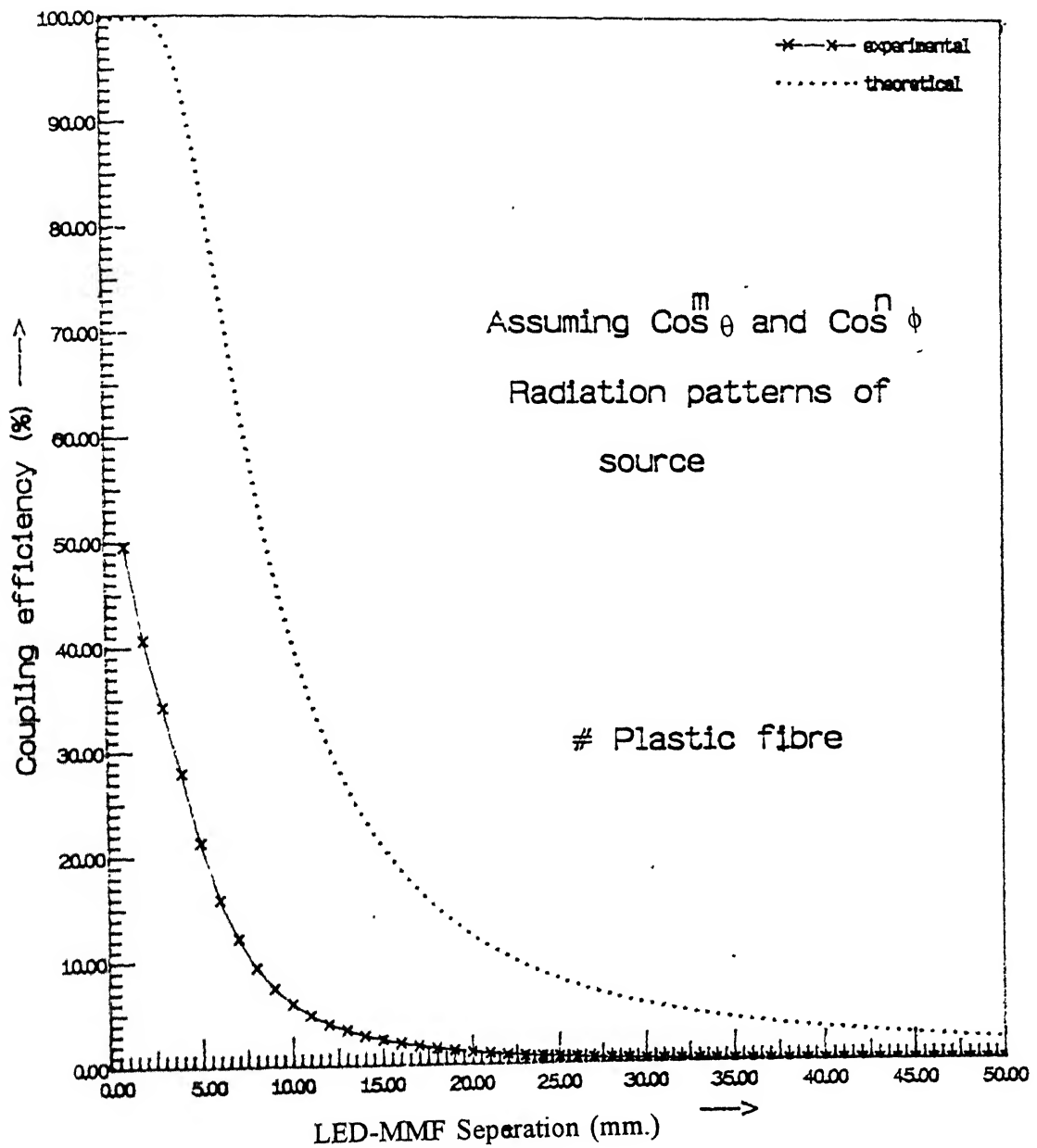Far field patterns for the LED-source and both the plastic and glass fibres, have been

43

Figure 4.8   Comparison of measured coupling efficiency with the calculated one for longitudinal offset for plastic fibre (Model-2)
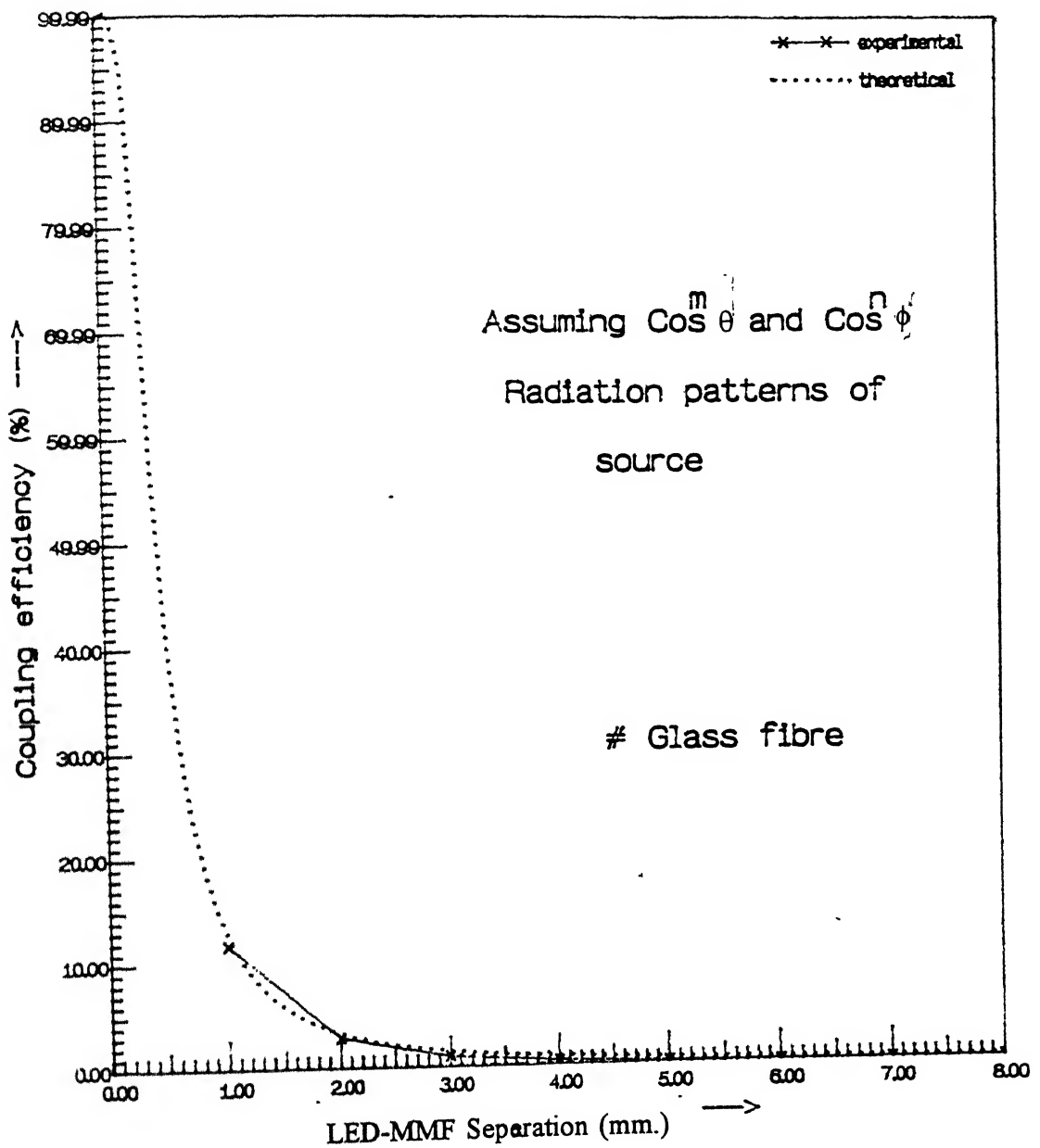
Figure 4.9 Comparison of measured coupling efficiency with the calculated one for longitudinal offset for glass fibre (Model-2)

obtained experimentally in chapter 3. Spot sizes W_{0x} and W_{0y} of the source and W_f of the fibre have also been calculated from these patterns by approximating the patterns to be gaussian This model has been referred as Model-3 in our theory.

For Butt coupling of two gaussian beams, the coupling expression given by eqn.(2.39) for both x and y directions can be used. The total coupling efficiency is then given by the geometric mean of η_x and η_y

$$n_x = \frac{4}{(\dfrac{W_{0x}}{W_f} + \dfrac{W_f}{W_{0x}})^2 \ [1 + (\dfrac{2z}{k \ (W_{0x}^2 + W_f^2)})^2]} \qquad (4.23)$$

$$n_y = \frac{4}{(\dfrac{W_{0y}}{W_f} + \dfrac{W_f}{W_{0y}})^2 \ [1 + (\dfrac{2z}{k \ (W_{0x}^2 + W_f^2)})^2]} \qquad (4.24)$$

As shown in ref. [10], the number of modes propagating in a fibre(M) is given as

For step-index fibre,

$$M = \frac{V^2}{2} \qquad \text{4.25(a)}$$

For graded-index fibre,

$$M = \frac{\alpha}{\alpha + 2} \cdot \frac{V^2}{2} \qquad \text{4.25(b)}$$

Since the amount of power that can be coupled into a fibre from an LED is limited by the product of LED coupled power per mode and the number of fibre modes[16], the total coupling efficiency can be calculated using eqn.(4.5). (4.23)-(4.25) as,
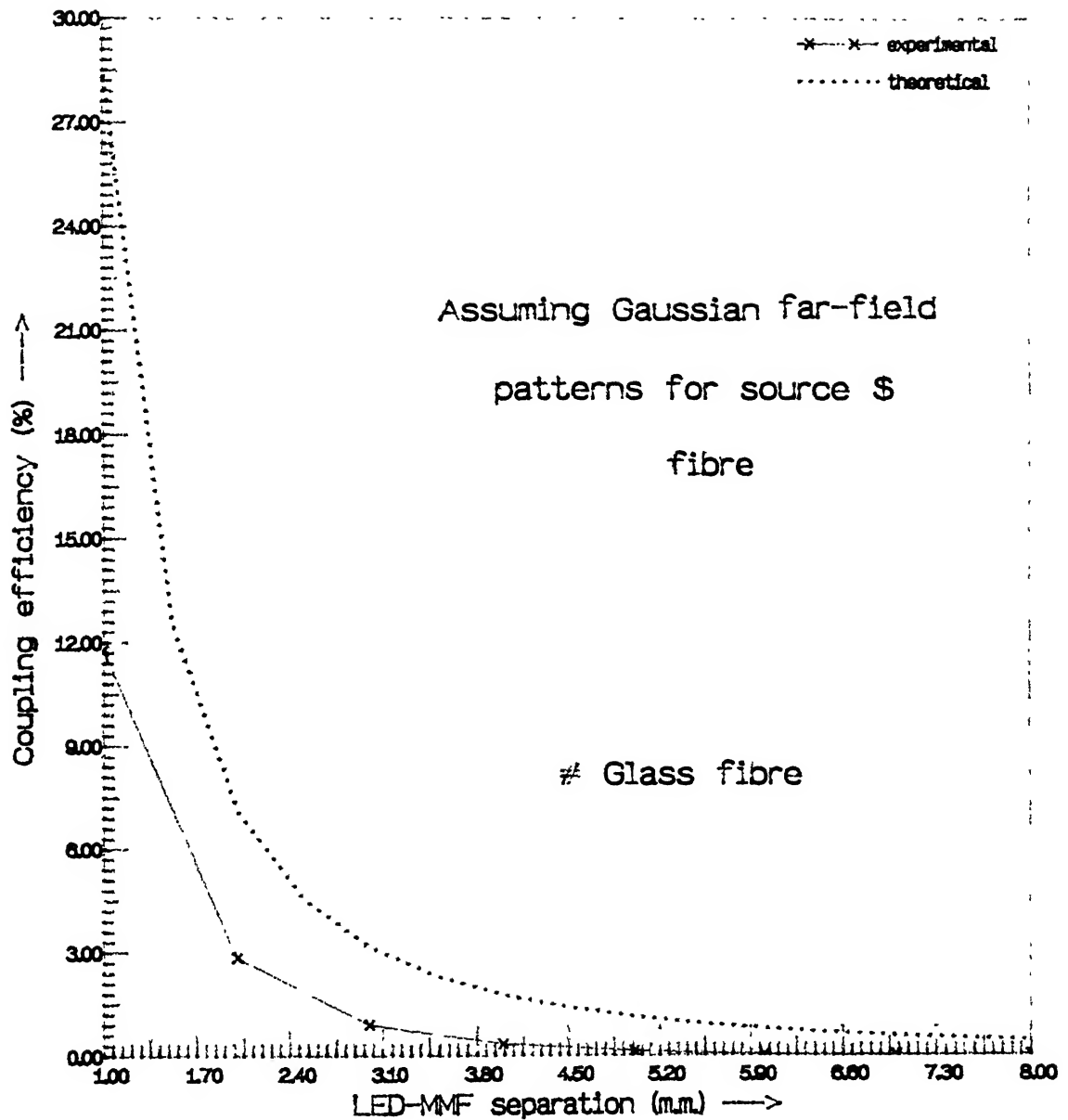
Figure 4 10 Comparison of measured coupling efficiency with the calculated one for longitudinal offset, for glass fibre (Model-3)

$$\eta = M \cdot (\eta_x \, \eta_y)^{1/2} \qquad\qquad (4.26)$$

Each mode is assumed to have the same power from the LED

Theoretical coupling efficiency for different values of longitudinal offset is calculated and plotted with experimental results for glass fibre See fig (4.10) Results are in quite good agreement and has been further discussed in the next section However, for plastic fibres, the assumption of equal power in all the modes may not be valid due to the very many number of modes propagated in the fibre

4.5 Comparisons of LED-MMF Coupling Theories in the Presence of Longitudinal Offset

Theoretical computations of LED to MMF coupling for butt case are carried out using uniform modal power distribution of LED source (Model-1), assuming $Cos^m \theta$ and $Cos^n \phi$ distributions of source (Model-2) and, assuming gaussian far-field patterns for LED source and fibres (Model-3). Experimental results for plastic and glass fibre, with LED as a source, are compared with the simulations. The coupling efficiency is found experimentally as the ratio of the power coupled into a short length of multi-mode fibres (measured using a power meter at the free end of the fibre) to the total power emitted by the source (measured using the same power meter). As the actual location of LED emitting region was not available, we assumed it to be 1 mm. from its glass enclosure. This put a limitation on the minimum longitudinal distance possible. If we extend our coupling efficiency graphs further to take into consideration this minimum separation, we see from fig.4.4 and 4.5 that experimental coupling efficiency of 60% and 30% are possible for plastic and glass fibre respectively.

With model-1, measured results are in good agreement with the theoretical ones, for plastic fibre But for glass fibre, experimental results exceed the theoretical ones just after a few mms. of LED-MMF separation. The reasons for the discrepancy in results are not very clear at the moment. One reason might be the presence of cladding modes in the short fibre lengths used Cladding modes could not be removed in our experiments. Another reason may be that the power is not uniformly distributed, rather concentrated more in the centre. For the sake of simplicity it could not be considered Also the models used in our studies are approximations

Experimental and theoretical results using model-2 are in very good agreement for glass

fibres. Model-2 theory is based on the parameters obtained from the measured radiation patterns Hence this model is expected to give the best results, as may be obtained from fig 4.9 However, for the plastic fibre, theoretical coupling efficiencies are much higher than the measured ones. One possible reason for smaller experimental results may be due to fibre end-faces not being well clean, smooth and perpendicular to the fibre axis It was not possible to make accurate experimental measurement due to the non-availability of good micropositioners. The overall accuracy may be of the order of 50-100 μm, which is not sufficient for the present study Theoretical coupling efficiency in all the models may also reduce, if Fresnel losses are included in the calculations.

With model-3, measured and calculated results are well matched for glass fibre as shown in fig 4.10. For plastic fibres, the theoretical results are found to be too optimistic, hence has not been presented here. This model using gaussian approximation of far-field pattern should be used only for fundamental modes of source and fibres. Since different amounts of power are coupled into different modes of the fibre, assumption of equal power coupling into each mode may not give accurate results.

From above models, we can conclude that the model-2 using $Cos^m \theta$ and $Cos^n \phi$ distributions of the source gives the best results for the glass fibre, and the model-1 using uniform modal power distribution for plastic fibres.

Summary

LED-MMF coupling theory has been simplified using various models (Uniform modal power distribution of source output, $Cos^m \theta$ and $Cos^n \phi$ distributions of source, and gaussian far-field patterns for the source and fibre). Experimental results have been compared with the modelled ones. Model-2 has been found to be the best

Chapter - 5

Conclusions and Suggestions for Future Work

The present work is aimed at studying the source to fibre coupling. The butt coupling efficiency for laser diode (LD) to single-mode fibre (SMF) is small (≈15%). The means by which LD-SMF coupling efficiency can be made close to 100%, are investigated. Hyperbolic microlenses are found to be the ideal in terms of achieving high coupling efficiencies Coupling theory for such microlenses is presented using finite-width phase shifter model and wave aberration model, followed by the misalignment theory. Gaussian approximation for the laser diode beam and weakly guiding step-index single-mode fibre has been assumed Reflections from the SMF end-faces are neglected without losing much accuracy. For typical SMF refractive indices, Fresnel's transmission coefficient yields around 0 96, thereby justifying the above approximations. The finite-width phase shifter model for hyperbolic microlenses doesn't give accurate results. This model gives good results for microlenses with smaller widths However, alignment tolerance is found to be more with this model. The wave aberration model is expected to give accurate results for wide microlenses because of its ability to consider lens aberration. However, the transverse alignment tolerances predicted using this model is much less than the previous one. This latter theory predicts higher coupling efficiency than the FWPS model. We conclude that the wave aberration model must be used to model microlenses, such as hyperbolic microlenses.

In case of LED-MMF coupling, the far-field patterns of source and multi-mode fibres are measured to obtain sum of their parameters. The LED-MMF butt coupling theory (longitudinal offset) with three simple models has been presented. Model-1 assumes the emitted power to be uniformly distributed in the elliptic cross-section of LED divergent beam, model-2 assumes $\cos^m \theta$ and $\cos^n \phi$ radiation patterns for the source, while model-3 considers gaussian far-field pattern for the source and fibres (plastic and glass) on the basis of the agreement between theoretical and experimental results It is concluded that model-1 suits best for plastic fibres while model-2 is ideally suited for glass fibres

In order to improve coupling efficiency, microlenses were formed on the endfaces of multi-mode fibres, using an optical glue. Microlensed coupling results were compared with the butt coupling ones for longitudinal and lateral offsets Microlens formation on fibres improved coupling efficiency but adversely affected their alignment tolerances.

Suggestions for Future Work

We have given three simple models to calculate LED-MMF coupling efficiency for longitudinal offsets. These models may be further extended for other misalignments i e lateral and angular offsets.

We have formed microlenses on the endfaces of multi-mode fibres and compared the measured results with butt coupling ones, for longitudinal and lateral offsets. For microlensed MMFs, coupling theory was not given due to the complexities involved Some simple models can be considered for these microlensed fibres and compared with our measured results. Some reliable (repeatable) methods for microlens formation may be investigated

REFERENCES

1   BARNOSKI,M.K., *Fundamentals of optical fiber communications*, Academic Press, chapters 1,2

2   BOTEZ,D. "Near and far-field analytical approximations for the fundamental mode in symmetric waveguide DH lasers ", *RCA Review*, Vol.39, Dec.1978, pp.577-603.

3   CHERIN,A.H., *An Introduction to Optical Fibres*, Mc Graw-Hill, 1983, Chaps.2,3,5

4.   EDWARDS,C.A., PRESBY,H.M. and DRAGONE,C.R., "Ideal microlenses for laser to fibre coupling", *Journal of lightware Technology*, Vol.11, No.2,1993, pp. 252-257.

5   ESENSTEIN,G., and VITELLO,D., "Chemically etched conical microlenses for coupling single-mode lasers into single-mode fibres", *Applied Optics*, Vol.21, No.19, Oct.1982, pp 3470-3474

6   FOA-1000, *Manual*, Serial No SN-F3068.

7   JOHN,G.A., "Microlenses to improve LED-to-fiber optical coupling and alignment tolerance", *Applied Optics*, Vol.18, No.21, 1 November 1979, pp.3694-3699.

8.   JOHN,J., "Semiconductor Laser Diode to single mode-fibre coupling using discrete and microlenses", *Ph.D. thesis*, university of Bermingham, January 1993.

9   JOHN,J., MACLEAN,T.S.M., H.GHAFOURI-SHIRAJ and NIBLETT,J., "Matching of single-mode fibre to laser diode by microlensesat 1.5 μm wavelength", *IEE Proc.-Optoelectronics*,Vol.141,No.3, June1994, pp.178-184

10. KEISER,G., *Optical Fiber Communications*, McGraw Hill, 2nd edition, 1991, chaps. 2,5.

11. KOGELNIK,H. and LI,T., "Laser beams and resonators," *Applied Optics*, Vol.5, No.10, Oct.1996, pp.1550-1567.

12. KOGELNIK,H., "Coupling and conversion coefficients for optical modes," *Proc.Symposium on Quasi-Optics*, Polytechnic Institute of Brooklyn, June 8 - 10, 1964, pp.333-347.

13. KUROKAWA,K., and BECKER,E.E., "Laser Fibre Coupling with a Hyperbolic Lens," *IEEE Trans. on Microwave Theory and Techniques*, March 1975, pp.309 - 311.

14. MURAKAMI,Y., YAMADA,J., SAKAI,J., and KIMURA,T., "Microlens tipped on a single-mode fibre end for InGaAsP laser coupling improvement," *Electronics Letters*, Vol.16, No.19, April 1980, pp.321-322.

15. NICIA,A. ,"Lens coupling in fiber-optic devices: efficiency limits ", *Applied optics*, Vol. 20, No.18, 15 Sept.1981, pp.3136-3145.

16. PERSONICK, S.D., *Optical Fibre Transmission Systems*, Plenum Press, Chap. 4.

17. PRESBY,H.M., BENNER,A.F., EDWARDS,C.A., "Laser micromachining of efficient fibre microlenses," *Applied Optics*, Vol.29, No.18, June 1990, pp.2692-2695.

18. PRESBY,H.M., and EDWARDS,C.A., "Near 100% Efficient Fibre Microlenses," *Electronic Letters*, Vol.28, No.6, March 1992, pp.477-484.

19 SAKAI,J., and KIMURA,T., "Design of a miniature lens for semiconductor laser to single-mode fibre coupling," *IEEE J. of Quantum Electronics*, Vol.QE-16, No.10, Oct.1980, pp.1059-1066.

20   SENIOR J.M., *Optical Fibre Communications*, Prentice Hall 1992, chaps. 2,7.

21.   YAMADA,J., MURAKAMI,Y., SAKAI,J., and KIMURA,T., "Characteristics of a hemispherical microlens for coupling between a semiconductor laser and single-mode fibre," *IEEE J. of Quantum Electronics,* Vol.QE-16, No.10, Oct.1980, pp.1067-1072.

EE-1995-M-GAR-STU